The *Drosophila* proventriculus lacks stem cells but compensates for age-related cell loss via endoreplication-mediated cell growth

Authors: Ben Ewen-Campen[1], Weihang Chen[1], Sudhir Gopal Tattikota[1], Ying Liu[1], Yanhui Hu[1], Norbert Perrimon[1,2]

Affiliations:

1. Department of Genetics, Blavatnik Institute, Harvard Medical School, Boston, MA 02115, USA
2. Howard Hughes Medical Institute, Boston, MA 02115, USA

Corresponding author: Ben Ewen-Campen and Norbert Perrimon
Email: bewencampen@genetics.med.harvard.edu, perrimon@genetics.med.harvard.edu

Abstract

The *Drosophila* proventriculus is a bulb-shaped structure at the juncture of the foregut and the midgut, which plays important roles in ingestion, peritrophic membrane synthesis, and the immune response to oral pathogens. A previous study identified a population of cells in the proventriculus which incorporate bromodeoxyuridine (BrdU), a marker of DNA synthesis, and proposed that these cycling cells are multipotent stem cells that replace dying cells elsewhere in the tissue. Here, we re-investigate these cycling cells and find that they do not undergo mitosis, do not generate clonal lineages, and do not proliferate in response to tissue damage, and are therefore not stem cells. Instead, we find that these cells continually endoreplicate throughout the fly's life, increasing their ploidy and cell volume, while at the same time nearby cells are lost into the gut lumen in an age-dependent process. These cells play a critical role in the synthesis of peritrophic membrane components, and we show that when endocycling in these cells is experimentally increased or decreased, nuclear and cellular volume as well as peritrophic membrane synthesis is concomitantly enhanced or reduced. Further, we show that blocking endocycling in these cells leads to functional defects in the peritrophic membrane, ultimately leading to increased susceptibility to orally infectious bacteria. Altogether, we show that continual endocycling of these cells is critical for maintaining tissue size and function over the course of the adult lifespan.

Introduction

The *Drosophila* gut is a highly regionalized organ with distinct functional domains along its length [1–3]. Within each domain, in addition to primary roles such as nutrient absorption and immunity, there are cellular mechanisms to ensure that the gut is repaired and renewed following tissue damage or cell loss. In the midgut, there are multipotent intestinal stem cells (ISCs) that continually divide to replace the differentiated cell types of the gut, both during homeostasis [4,5] and in response to tissue damage [6,7]. Analogous ISCs are present in the mammalian small intestine [8,9], which is functionally comparable to the *Drosophila* midgut [10].

In contrast to the midgut, in the hindgut there is no evidence of multipotent stem cells [11,12]. Instead, hindgut cells respond to tissue damage by undergoing extensive endocycling, a specialized cell cycle in which DNA is replicated without undergoing mitosis, thus increasing the ploidy and nuclear size of hindgut cells [11]. In *Drosophila*, this endocycling response to tissue damage or wounding is conserved in the adult epidermis [11,13,14], and is important to maintain tissue integrity in the absence of stem cell activity.

At the anterior of the gut, where the foregut meets the midgut, there is a specialized bulb-shaped structure called the proventriculus (also known as the cardia, based on its shape). A previous study [15] identified a ring of cells in the proventriculus which incorporate the nucleotide analog BrdU, a marker of S phase, and proposed that these cycling cells are stem cells that replace dying cells elsewhere in the proventriculus.

Here, we re-investigate the function of these previously-identified cycling cells in the proventriculus. We find no evidence that these cells undergo mitosis, generate clonal lineages, or respond to tissue damage, either by mitosis or by increasing endocycling. Instead, we find that these cells continually endocycle throughout the fly's life, at a rate that varies with systemic nutritional signals. Further, we find that cells from this region of the proventriculus are progressively lost into the gut lumen as the fly ages, and the remaining nuclei and cells become progressively larger in volume via endocycling. Lastly, we use functional studies to show that blocking endocycling in these cells disrupts peritrophic membrane formation, whereas inappropriately enhancing endocycling leads to increased peritrophic membrane formation. We conclude that the proventriculus does not contain stem cells, but that it instead compensates for age-related cell loss by endocycling-mediated cell growth to maintain tissue function.

Results and Discussion

The proventriculus contains a ring of cycling cells in Zone 4. The proventriculus consists of a doubly-folded tubular epithelium and associated muscles and neuronal structures (Figure 1A) [16–18]. It forms during embryogenesis by the invagination of an anterior, ectodermal portion of the embryonic gut (the future esophagus) into an adjacent segment of endodermal gut, creating a bulb structure with an internal lumen [19–21]. In addition to serving as a muscular valve surrounding the esophagus, the proventriculus plays a critical role in the synthesis of the peritrophic membrane [16–18]. Studies in other Dipterans have shown that the proventriculus is capable of producing peritrophic membrane at a rate exceeding six mm/hour at 25ºC, representing an enormous capacity for synthesis and secretion [22,23]. In addition to peritrophic membrane synthesis, the proventriculus plays important roles in the immune system [24,25], and as a site for regulation of the microbiota [26].

Morphological studies have identified six distinct "zones" arranged linearly along the proventriculus epithelium, based upon cellular morphology and on their proposed role in the synthesis of the peritrophic membrane [16]. These anatomical zones have been shown via single cell RNAseq (scRNAseq) to largely correspond to transcriptionally distinct cell types [25].

Zone 4 is a ring-shaped structure that encircles the esophagus at the anterior of the proventriculus (Figure 1A). A previous study identified a ring of cells located at the posterior limit of Zone 4 which consistently incorporate BrdU, indicating that these cycles progress through S phase in adult flies [15]. This study proposed that these cycling cells are multipotent stem cells that proliferate and replace dying cells elsewhere in the proventriculus [15].

Functionally, Zone 4 cells are highly secretory and play an important role in the synthesis of chitin and other peritrophic membrane components [16,25,27]. scRNAseq studies indicate it is enriched for genes involved in chitin synthesis and chitin modifications, including *chitin synthase 2 (chs2) [25]* which can be visualized with *chs2-Gal4 > UAS:2XEGFP* (Figure 1B, left). Studies in larval flies confirm that mutations in *chs2* lead to defects in peritrophic membrane synthesis [27], and visualizing the peritrophic membrane with fluorescent HPA lectin [28,29] confirms previous observations that peritrophic membrane components is highly enriched in the lumen

directly abutting Zone 4 cells (Figure 1B, middle.) Zone 4 cells also express high levels of the WNT pathway ligand Wingless (Figure 1C, right), as reported by [15].

To re-investigate the function of these cycling cells, we fed flies with EdU for two days and confirmed the presence of a ring of EdU+ cells at the posterior edge of Zone 4 (Figure 1C, left). EdU+ cells are occasionally observed elsewhere in the proventriculus (see e.g. Figure 1G, 2A), but here we focus exclusively on the EdU+ population in Zone 4. Previous studies suggested that, in addition to Wg expression, JAK-STAT signaling is also enriched in this area [15], and when we co-labeled proventriculi for EdU and 10XSTAT:GFP, a JAK-STAT pathway reporter, we found that the EdU+ population is directly anterior to STAT+ cells, suggesting that EdU+ cells are enriched at the posterior edge of Zone 4, with 10XSTAT expression representing the anterior limit of Zone 3 (Figure 1C, right).

To characterize the dynamics of EdU incorporation over time, we fed flies with EdU for 1, 3, or 5 days. We performed this experiment with two standard lab genotypes, w^{1118} and *OreR,* and observed that the number of labeled cells increased linearly with time (Figure 1D), at a rate of between 3.3 (w^{1118}) and 4.1 (*OreR*) EdU+ cells per day, suggesting that cells in this region are continually entering S phase at a relatively constant rate.

To test whether individual cells cycle continuously over time or whether they cease cycling after a discrete number of S phases, we performed an EdU pulse-chase experiment by feeding EdU for 3 days, followed by a 20 day chase in the absence of EdU (Figure S1). After 20 days, we observed a marked decrease in EdU+ cells in Zone 4, suggesting that the EdU signal was diluted by continued cycling (Figure S1). This dilution over time is similar to what is observed for the continually cycling ISCs (mitotic) and enterocytes (ECs; endocycling) of the posterior midgut (Figure S1), and contrasts with what is observed in the hindgut, where BrdU signal is retained for 20 days due to a lack of continual cycling under homeostasis [11].

In these initial observations, we noted progressive changes in the nuclear morphology of EdU+ cells. Specifically, after 1d of EdU feeding, Edu+ nuclei tended to be small in volume and located at the posterior limit of Zone 4 (Figure 1D, left) whereas after 5d of feeding labeled nuclei were larger and could be seen a few cell diameters anteriorly (Figure 1D, right). This increase in nuclear size suggests that EdU+ incorporation in these cells may reflect an increase in genomic size via endocycling, a modified cell cycle in which cells become polyploid by replicating DNA without undergoing mitosis or cell division, rather than mitotic activity as previously suggested.

It has previously been shown that systemic nutritional signals tightly correlate with endocycle progression in a variety of cellular contexts in the *Drosophila* larva, whereas mitotic activity is not clearly linked to nutritional status [30,31]. We tested whether the EdU+ cells in Zone 4 are responsive to nutrition by varying the amount of dry active yeast, a primary source of protein and other macronutrients for *Drosophila*, added to a standard minimal lab food (see Methods). We found that the number of EdU+ cells increased in direct proportion to the amount of yeast

147 added to the fly's food (Figure 1E), suggesting that the cycling of these cells is influenced by
148 systemic nutritional cues.
149
150 We further tested this sensitivity to systemic nutrition using a genetic tumor model in the midgut
151 (*esg-Gal4, tubGal80^{ts} > UAS:yki^{3SA};* note that *esg-Gal4* is not expressed in the proventriculus),
152 which promotes systemic muscle wasting and cachexia via the upregulation of the systemic
153 insulin antagonist *Impl2,* the cytokine *upd3,* and other cytokines [32–34]. In cachectic flies, we
154 observed a significant decrease in the number of Zone 4 cells labeled with EdU+ (Figure
155 S2A,B), indicating that cycling in the cells is directly responsive to systemic reduction in insulin
156 signaling. We then tested whether over-expressing the insulin antagonists *Impl2, upd3*, or both
157 together, would lead to a similar reduction in EdU+ cells in the proventriculus. Indeed, when we
158 expressed these factors from other ISCs (*esg-Gal4*) or from muscles (*dMef2-Gal4*), both of
159 which decrease systemic insulin signaling, we observed a significant decrease in EdU+ cells of
160 the proventriculus (Figure S2A,B).
161
162 Altogether, these observations confirm that the adult proventriculus contains a ring of cells at
163 the posterior of Zone 4 which consistently cycle through S phase, and that they do so in
164 response to systemic nutritional signals. Further, initial observations of their cellular morphology
165 over time suggests that they may be endoreplicating rather than undergoing mitosis.
166
167 **A molecular atlas and Gal4 toolkit for functional studies of the proventriculus.** In order to
168 functionally characterize these EdU+ cells *in vivo*, we generated a toolkit of Gal4 lines to label
169 and manipulate various cell types of the proventriculus. First, we screened the K-Gut database
170 [35] for Gal4 lines that specifically label Zone 4. We identified four lines that labeled Zone 4,
171 inclusive of EdU+ cells, (GMR41F06-GAL4, GMR26D04-GAL4, GMR56D02-GAL4, and
172 GMR71F06-Gal4) and selected a particularly specific and consistent line, 71F06-Gal4, for
173 further study (Figure 2A).
174
175 Next, to identify molecular markers for other proventriculus cell types and to serve as a
176 foundation for further molecular study, we created a single cell transcriptional atlas of the
177 proventriculus using single nucleus RNAseq (snRNAseq). We sequenced a total of 22,332
178 nuclei from approximately 600 dissected proventriculus tissues, which ultimately resolved into
179 14 transcriptionally-defined clusters (Figure 2B,C,D). This atlas is available via an online data
180 portal (https://www.flyrnai.org/scRNA/).
181
182 We mapped the identity of these snRNAseq clusters to *in vivo* anatomy using cluster-specific
183 marker genes. One cluster was enriched for molecular markers of muscles (e.g. *Mhc, up*) and
184 two clusters were enriched for pan-neuronal markers (e.g. *nSyb, elav, brp*), one of which was
185 enriched for *Akh-* and *Impl2*-expressing cells and therefore likely represents the corpora
186 cardiaca [36–38]. To map the remaining 11 clusters to the *in vivo* proventriculus, we examined
187 the expression of top marker genes for each cluster using either Gal4 lines or split-intein Gal4
188 lines crossed to a ubiquitous reporter (Figure 2C,D,E.) [39].
189

190 We were able to identify the remaining clusters as anatomically distinguished epithelial cell
191 types. One cluster corresponded to the esophagus (marked by *Elovl7-Gal4*), another to Zone 1
192 (marked by *CG11550-Gal4* and *Cht7-Gal4*). At the clustering resolution we selected, Zone 2
193 and 3 cells were both found in a single cluster (enriched for *Ppn-Gal4* and *Cyp49a1-Gal4*). We
194 observed a distinct cluster enriched for *Lgr1* and *Delta* that corresponds to a population of cells
195 specifically at the anterior border of Zone 3, immediately posterior to Zone 4. We recovered
196 distinct clusters corresponding to Zone 4 (*Wnt4-Gal4*) and Zone 5 (*Ca-Ma2d-Gal4*), as well as a
197 cluster that corresponds to a discrete band of cells at the widest diameter of the proventriculus,
198 at the border of Zone 5 and 6 (marked by *CG10702-Gal4, Notum-Gal4*, *Mco4-Gal4*$^{N\text{-}int}$). A
199 cluster enriched for *SecCl-Gal4* corresponded to Zone 6, and a cluster enriched *mex1-Gal4* and
200 *P5CS-Gal4* corresponded to the anterior midgut. Two additional minor clusters (labeled
201 "unknown" and "anterior midgut 1" in Figure 2B) were enriched for markers corresponding to
202 multiple cell types and were excluded from further analysis. In a previous scRNAseq atlas of the
203 *Drosophila* midgut [40], midgut ISC clusters were enriched for the stem cell marker *esg*, as well
204 as cell-cycle related genes *PCNA* and *stg.* Notably, we did not observe notable expression of
205 any of these genes, nor any cluster-specific enrichment for any *cyclin* genes, in our
206 proventriculus atlas, whether in our Zone 4 cluster or elsewhere.
207
208 Our snRNAseq atlas is largely concordant with a recently published scRNAseq atlas of the
209 proventriculus [25], with minor deviations in the proportions of cells present in each cluster
210 (Figure S3). This high degree of concordance suggests that these cell types we identify are
211 robust to experimental approach, as these two atlases were created using entirely different
212 single cell protols; Zhu (2024) sequenced single cells from freshly dissected and chemically
213 dissociated suspensions, while we sequenced isolated nuclei from flash frozen tissues. We also
214 note that our atlas was generated from two distinct biological samples: proventriculi from control
215 flies and from cachectic flies, and thus includes cells across a range of nutritional status (see
216 Methods). This snRNAseq atlas thus serves as a resource for studies of the proventriculus, and
217 allows us to identify cell type-specific Gal4 driver lines for functional experiments.
218
219 **No evidence for mitosis in the proventriculus.** Stem cells are defined as multipotent
220 precursor cells that undergo repeated asymmetric mitosis, giving rise to one daughter cell that
221 retains a stem identity and another daughter cell capable of differentiation. Thus, mitosis is a
222 critical feature of any stem cell system. A previous study of the proventriculus suggested that
223 rare mitoses do occur in this tissue, albeit at a rate that is seemingly out of proportion with the
224 steady numbers of cells passing through S phase [15].
225
226 To re-examine whether these cells undergo mitosis, we first stained guts from two different
227 control genotypes (20 *OreR* wildtype guts, 36 *71F06 > UAS:GFP* guts, total n = 56 guts) for
228 phosphorylated Histone 3 (pH3+), a marker of mitosis. We fed these flies colchicine overnight
229 prior to staining, which enriches for pH3+ cells by blocking exit from mitosis [11]. We observed
230 zero pH3+ cells in the epithelia of Zone 4 in these flies, or anywhere else in the proventriculus.
231
232 The cell cycle can be experimentally driven forward by over-expressing such oncogenes as
233 activated Yki or Ras, or by *Notch* loss-of-function, and in cells that are capable of mitosis these

manipulations will strikingly increase M phase. For example, in ISCs of the posterior midgut, over-expression of *UAS-yki*^{3SA} [41–43] or *UAS-Ras1*^{A} [44–46], or knock down of *Notch [5,47]* all lead to dramatic over-proliferation via excess mitosis, leading to massive tumor growth. We hypothesized that, if Zone 4 cells are competent to undergo mitosis, over-expression of such cell cycle promoting factors should lead to an increase in mitotic cells.

To test whether these factors can drive mitotic proliferation in the proventriculus, we used *71F06-Gal4* to drive *UAS-yki*^{3SA}*, UAS-Ras1*^{A}*,* or *Notch-RNAi* in Zone 4 cells. These manipulations caused a dramatic enlargement of Zone 4, increased cytoplasmic extrusions into the gut lumen (Figure 3 and S4A,B), and a expansion of the domain that typically incorporates EdU to cover the entire Zone 4 rather than a band at its posterior edge (Figure 3A). However, we did not observe a single pH3+ cell under any of these conditions, which also included colchicine treatment to enrich for pH3+ (Figure 3B). As a positive control, imaging the posterior midguts from these same samples showed extensive pH3+ staining (Figure 3B).

These results demonstrate that EdU+ cells located in Zone 4 of the proventriculus do not undergo mitosis either under homeostatic conditions or when experimentally driven through cell cycle progression via ectopic oncogene expression. Furthermore, we note that despite morphological deformities caused by over-expressing activated Yki or Ras1, we never saw these cells travel from Zone 4 into any other portion of proventriculus, which provides further evidence that EdU+ cells in Zone 4 are not capable of replacing damaged or dead cells in other regions of the tissue as suggested by [15].

No evidence for clonal growth of Zone 4 cells in the adult proventriculus. Despite the absence of pH3 staining, it is possible that rare mitoses occur. Another hallmark of adult stem cells is the ability to generate multipotent clones in the adult organism. For example, in the adult posterior midgut, MARCM-based lineage tracing of ISCs leads to the presence of GFP-labeled clones throughout the midgut that contain all of the epithelial cell types that can be generated by ISC differentiation [5,47]. We therefore used MARCM-based lineage tracing to test whether there is clonal growth in the adult proventriculus.

As a positive control for our labeling protocol, we heat-shocked MARCM19A larvae during the L3 larval stage, when this tissue is still undergoing developmental proliferation. We observed large GFP+ clones throughout the proventriculus, both in Zone 4 and elsewhere, in every sample examined, demonstrating that MARCM labeling functions as expected in this tissue (Figure 4A). As a negative control, we examined GFP+ patterns in both midguts and proventriculi from non heat-shocked flies, and observed small numbers of scattered GFP+ cells throughout the proventriculus, as well as in the midgut. We scored proventriculi as having either no GFP+ clones, between 1-5 small groups of GFP+ cells (typically 1-2 cells each), or having large GFP+ clones that include >10 cells (Figure 4D).

To test for clonal growth during the adult stage, we heat-shocked MARCM19A flies several days after eclosion, then reared them for varying lengths of time before scoring for GFP+ clones. We

277 challenged an additional cohort of flies with a 2-day starvation followed by re-feeding, which
278 increases ISC proliferation in the midgut [48,49].
279
280 As expected, in the posterior midgut we observed GFP+ clones in the midguts of heat-shocked
281 flies after 14 days, and we also found that these clones tended to be larger in flies that
282 experienced a 2 day starvation (Figure 4B). In contrast, in the proventriculus of these flies,
283 observed scattered singlet and doublet GFP+ cells throughout the tissue at roughly similar rates
284 between negative controls and heat-shocked flies (Figure 4C,D). This was true at 14 days after
285 heat-shock, 19 days after heat-shock, and 30 days at 18ºC after heat-shock (Figure 4C,D).
286
287 In the midgut, ISCs divisions increase dramatically upon tissue damage [6,7]. To test whether
288 there may be damage-responsive proliferation in the proventriculus, we repeated these MARCM
289 experiments in flies subjected to a variety of damage: bleomycin treatment, infection with
290 pathogenic *ECC15* bacteria, and 2000 RADs of X-rays [6,7]. Given that we observed that EdU+
291 incorporation increases with additional yeast content, we also performed MARCM experiments
292 with 10% yeast supplementation. We did not observe discernable GFP+ clones emanating from
293 Zone 4 or any other area of the proventriculus in any of these conditions (Figure S5). We note
294 that, unlike enterocytes of the midgut, Zone 4 cells do not directly contact the contents gut
295 lumen and therefore likely do not experience damage to the same extent as ECs, but
296 nonetheless we did not observe GFP+ clonal growth under any of these conditions. Altogether,
297 we find no evidence for clonal growth of the EdU+ cells in Zone 4 of the proventriculus.
298
299 **Zone 4 cells do not cycle or proliferate in response to apoptotic damage in the**
300 **proventriculus.** In the midgut, ISCs proliferate at low levels under homeostatic conditions, and
301 increase proliferation in response to tissue damage and/or dying enterocytes [6,7]. In contrast,
302 in the hindgut, cells do not mitotically proliferate in response to damage but instead undergo
303 extensive endoreplication [11,12]. A previous study in the proventriculus suggested that the
304 EdU+ population of cells in the proventriculus proliferates in order to homeostatically replace
305 dying cells elsewhere in the tissue [15].
306
307 To directly test how the EdU+ population of cells responds to nearby tissue damage, we used
308 the Gal4-UAS system to induce cell death in various cell types of the proventriculus by over-
309 expressing the proapoptotic factor *UAS-RPR*. We drove cell death in three different cell types of
310 the proventriculus: in Zone 5 (*Ca-Ma2d-Gal4*), in Zone 1 (*CG11550-Gal4*), and in the
311 esophagus (*Evolv7-Gal4*) (Figure 4). In these experiments, we silenced *UAS-RPR* throughout
312 development using *tubGal80*^{ts} and raising flies at 18ºC until several days post-eclosion, and
313 then activated tissue damage by shifting adult flies to 29ºC for 48 hours. We placed flies on
314 EdU-containing food for the duration of the tissue damage, and throughout a recovery phase of
315 2 days or 5 days at 18ºC following damage. If these EdU+ cells in Zone 4 proliferate to
316 compensate for dying cells, we would expect to see an increase in EdU+ cells in response to
317 damage, and likely EdU+ cells growing towards the area of damage.
318
319 We observed pyknotic nuclei, indicative of apoptosis, in the intended cell type in *UAS-RPR* flies,
320 and not in control flies (Figure 5A, B, C), indicating that this system induces apoptosis as

expected. However, in all three experiments we observed not an increase in EdU+ cells, but rather a significant decrease (Figure 5.) These results are inconsistent with the hypothesis that these cells proliferate in response to tissue damage elsewhere in the proventriculus. The decrease in EdU+ cells in all cases further supports the previous observation that these cells cycle in response to systemic cues indicative of organismal health.

Interestingly, when we drove apoptosis in the esophagus with *Elovl7-Gal4*, while we observed a decrease in EdU+ cells in Zone 4, we did observe indications of massive endoreplication in the esophagus itself: unusually large, EdU+ nuclei (Figure 5C, asterisks). This is similar to what has been reported in the hindgut [11], and we note that both the foregut and hindgut are ectodermal in origin [50]. In contrast, the remainder of the proventriculus, like the midgut proper, is endodermal in origin and we did not observe any similar indications of endoreplication in the damaged tissue (Figure 5A,B). We thus propose that damage-responsive endoreplication may be a phenomenon primarily found in ectodermally-derived tissues, and note that it is also observed in the epidermis which is ectodermal in origin[11,13,14].

Genetic lineage tracing using a highly specific split-intein Gal4 line that labels EdU+ cells in Zone 4. As an additional method for lineage tracing independent of MARCM, we wished to genetically label the descendants of Zone 4 EdU+ cells using a Gal4 line specific to these cycling cells. However, we did not observe any discernible transcriptional signatures of the Zone 4 EdU+ cells, and were initially unable to identify a Gal4 driver to specifically label these cells within Zone 4.

We thus used the split-intein Gal4 system to generate a genetic driver that specifically labels the EdU+ population of cells in Zone 4 [39]. We generated a split-intein Gal4$^{N\text{-}int}$ line using the 71F06 enhancer fragment that drives expression in Zone 4 (Figure 5A), and then used our snRNAseq atlas to identify *Delta* as a candidate gene which is primarily enriched in Zones 1-3 and in Zone 3-4 border cells, with some expression as well in Zone 4 (Figure 6A). When we examined the intersectional labeling of *71F06-Gal4::Gal4-C-int ∩ Delta*$^{Gal4\text{-}N\text{-}int}$ *> UAS:2xEGFP*, we observed strikingly specific expression in a band of cells at the posterior edge of Zone 4 (Figure 6A). We confirmed that these cells contain the large majority of EdU+ cells (Figure 6B).

To lineage trace these cells, we used the G-TRACE system combined with *tubGal80*^{ts}, which labels current expression in RFP and lineage expression in GFP [51]. After development at 18ºC, we placed *71F06-Gal4::Gal4-C-int ∩ Delta*$^{Gal4\text{-}N\text{-}int}$ *, tubGal80*^{ts} *> G-TRACE* at 29ºC to initiate lineage tracing and examined the proventriculus after 1 day, 6 days at 10 days (Figure 6C,D). If these cells are proliferating and generating clones, we would expect to see progressively larger areas of GFP+ / RFP- cells as descendants of these cells grow into the rest of the tissue. However, while we did observe small numbers of GFP+ / RFP- cells immediately adjacent to the GFP+/RFP+ domain, the number of these cells did not increase or move over time, but were constant over a 10 day period (Figure 6C,D). These results are consistent with leaky and/or minor dynamic changes in the expression pattern of our split-intein Gal4 line, rather than with proliferation of cells in this domain.

364
365 Taken all together, we find no evidence that the EdU+ cells located in Zone 4 are stem cells.
366 We do not observe mitosis, nor the generation of MARCM clones, nor a proliferative response
367 to nearby tissue damage, nor any evidence of genetic cell lineages growing over time. We thus
368 propose that these cells must be endocycling through a cell cycle that lacks an M phase.
369
370 **Zone 4 cells progressively increase in ploidy over the fly lifespan, as others are lost into**
371 **the lumen.** The consistency with which EdU is incorporated into cells in Zone 4 suggests that
372 these cells are continually endocycling throughout the fly's life and thus increasing in ploidy.
373 Indeed, microscopy-based ploidy analysis [52] of Zone 4 cells indicated a wide range of ploidy
374 states, with the majority between 4N and 16N, and including cells up to 40N (Figure S6).
375
376 If this cell cycling reflects consistent endocycling throughout the fly's life, these cells should
377 progressively increase in nuclear volume as flies age [31,53]. To test this directly, we performed
378 a time-course experiment using confocal microscopy to quantify the number and volume of
379 Zone 4 nuclei over the course of fly aging. In this experiment, *71F06-Gal4 > UAS:GFP*^{stinger} flies
380 (hereafter, *UAS:GFP*^{NUC}), which express nuclear-localized GFP in Zone 4, were split into vials
381 either containing dried active yeast powder *ad libitum* or standard food lacking additional yeast
382 powder, and were examined at six timepoints between 3 days and 35 days after eclosion. At
383 each time-point, we collected 5 confocal z-stacks and quantified both the number of GFP+
384 nuclei as well as the 3D volume of these nuclei (Figure S6A).
385
386 We observed a consistent, monotonic increase in nuclear volume over the course of the fly's
387 life, supporting the hypothesis that these cells are endocycling and thereby increasing in ploidy
388 (Figure 7A,B,C). Consistent with the observation that supplemental yeast increases EdU
389 incorporation, we found that nuclear volume increased more quickly in flies which received dried
390 active yeast, but that by 28 days the average nuclear volume was not significantly different
391 between these treatments (Figure 7A,B,C). As an internal comparison, we also quantified the
392 volume of diploid ISCs from these same guts and using the same volume quantification pipeline.
393 At 3d after eclosion, many Zone 4 nuclei were approximately the same volume as diploid ISCs
394 (Figure S6B). Over the course of the fly's life, nuclear volume increased until at 35 days old the
395 largest nuclei were ~16X larger in volume than diploid ISCs (Figure S6B). Co-staining these
396 samples with the f-actin marker phalloidin indicated that Zone 4 cells remain mononucleate,
397 even at the latest time point (35d) when the tissue begins to lose a clearly monolayered
398 epithelial structure (Figure S6C).
399
400 Surprisingly, we observed that while the volume of Zone 4 nuclei progressively increased, the
401 total number of nuclei steadily decreased (Figure 7D). Over the first 14 days, cell numbers
402 decreased at equivalent rates for flies fed with or without yeast, but beginning at 21 days the
403 number fell faster for flies without added yeast (Figure 7D). Remarkably, throughout this time-
404 course, we observed that GFP+ nuclei were being shed into the gut lumen (Figure 7E,F and
405 S7). We quantified the number of GFP+ nuclei present in the lumen outside the Zone 4
406 epithelium, representing a snapshot of cell loss at the time of dissection, and found that the
407 number of cells shed into the lumen first started to increase at 14 days after eclosion, and

408 subsequently increased until reaching a maximum at 28 days (Figure 7D). The mechanism by
409 which these cells exit the epithelium is not known, but we observed holes forming in the F-actin-
410 rich barrier separating Zone 4 cells from the gut lumen, with GFP+ nuclei passing through these
411 holes into the lumen (Figure S7). We note that the patterns of cell loss correspond neatly with
412 our total cell counts, with the greatest decreases in cell numbers corresponding to those time-
413 points when more nuclei were being lost.
414
415 Together, these data suggest that Zone 4 nuclei are endocycling and thus increasing in ploidy
416 and nuclear volume at the same time that cells from this region are being lost into the lumen.
417 One simple explanation for these observations is that genomic copy number is increasing in
418 order to maintain metabolic output and tissue integrity as cells are progressively lost during
419 aging.
420
421 **Disruptions to endocycling in Zone 4 lead to altered peritrophic membrane synthesis and**
422 **function.** Increasing genomic copy number is a widespread mechanism to enhance synthesis
423 of proteins and other biological components in non-proliferative tissues [31,53,54]. Given the
424 role that Zone 4 cells play in the synthesis and secretion of chitin and other peritrophic
425 membrane components [25,27], we hypothesized that endocycling in this tissue is linked to
426 peritrophic membrane synthesis. We therefore used genetic manipulations to both increase and
427 decrease endocycling, and then visualized the peritrophic membrane and tested for functional
428 defects.
429
430 To increase endocycling, we overexpressed *UAS:CycE* or *UAS:Myc* in Zone 4 cells using
431 71F06-Gal4. CycE is a key regulator of both endocycling and the mitotic cell cycle, and drives
432 entry into S phase [31,55], and Myc is a transcription factor whose overexpression is sufficient
433 to drive endocycling and increased nuclear volume in many contexts [31,54,56,57]. In Zone 4
434 cells of the proventriculus, both of these manipulations led to increased EdU incorporation and
435 the formation of significantly enlarged nuclei after 7-9 days at 29ºC (Figure 8A, B and S9A). We
436 visualized the peritrophic membrane formation using HPA lectin staining, and observed
437 enlarged streams of glycosylated material emanating from Zone 4, forming thickened cords that
438 were not observed in controls. We interpret these to indicate that increased endocycling leads to
439 enhanced synthesis of peritrophic membrane components in Zone 4.
440
441 To inhibit endocycling, we noted that the cycling of these cells is highly dependent on nutritional
442 status. We therefore knocked down the insulin receptor (*InR*) in Zone 4, which mimics starvation
443 specifically in these cells. Using two independent RNAi constructs, we observed a near total
444 loss of EdU staining in *InR RNAi* animals after 6 and 15 days at 29ºC (Figure S9B,C) and a
445 concordant failure to increase in nuclear volume over time (Figure 8B). In control flies (w^{1118} or
446 *mCherry-RNAi*), Zone 4 nuclei steadily increase in nuclear volume between 6 days and 21 days
447 at 29ºC, where in *71F06-Gal4* > *InR-RNAi* flies, these nuclei did not increase in volume (Figure
448 8B). The overall size of Zone 4, visualized with cytoplasmic *UAS:2XEGFP,* was dramatically
449 reduced by *InR RNAi*, indicating that nuclear volume and overall cell size are linked, as
450 expected (Figure 8C.)
451

452 Visualization of the peritrophic membrane in *71F06-Gal4 > InR-RNAi* revealed notably less
453 material emanating from Zone 4, and overall far less visible peritrophic membrane within the
454 proventriculus (Figure 8D). Consistent with the reduced nuclear volume and tissue size, the
455 quantity of peritrophic membrane emanating from Zone 4 in these animals appeared to be
456 reduced and altered (Figure 8D). These alterations in peritrophic membrane morphology are
457 consistent with the hypothesis that increased genomic copies allow for increased synthesis of
458 peritrophic membrane components.
459
460 To assess the functional consequences of this reduction in peritrophic membrane production,
461 we assayed their resistance to orally-ingested pathogen infection. The peritrophic membrane is
462 a critical barrier to pathogens [58–60], so we hypothesized that reduced endocycling in Zone 4
463 cells may lead to functional defects in pathogen resistance. Under standard conditions at 29ºC,
464 the lifespan *71F06-Gal4 > InR-RNAi* flies was indistinguishable from control flies (Figure 8E).
465 However, when these flies were challenged with the pathogenic bacteria *Pseudomonas*
466 *aeruginosa* (*PA14*), *InR RNAi* flies were far more susceptible to infection than controls (Figure
467 8F). This is consistent with a compromised peritrophic membrane.
468
469 These experiments also allowed us to test whether endocycling-based cell growth was
470 functionally causal for the loss of cells from Zone 4 during aging. If cell loss was driven by the
471 process of tissue growth via endocycling, then experimentally increasing endocycling via *UAS-*
472 *Myc* or *UAS-CycE* should lead to enhanced less loss. We counted the number of GFP+ cells in
473 these genotypes one day after shifting to 29ºC, and after 12 days (Figure S10). The number of
474 cells in each genotype decreased after 12 days by between 21% - 31%, but the percent
475 decrease between genotypes were not significantly different (Figure S10), despite the fact that
476 nuclear volume is greatly increased in these genotypes compared to controls (Figure 8A,B,
477 Figure S8). This suggests that the shedding of Zone 4 cells during aging is not driven by
478 endocycling itself, and that a distinct mechanism must govern the loss of cells.
479
480 Altogether, these experiments demonstrate that endocycling leads to increased nuclear and
481 cellular volume, ultimately increasing the production of peritrophic membrane components.
482 Given the observation that under wildtype conditions, Zone 4 cells are lost over the course of a
483 fly's life, we propose that endocycling is a compensatory mechanism to ensure that continued
484 production of sufficient quantities of peritrophic membrane components.
485
486 **Conclusions.** We find no evidence of stem cells in the *Drosophila* proventriculus. The EdU+
487 cells in Zone 4 do not undergo mitosis, do not produce clonal lineages, and do not cycle in
488 response to nearby tissue damage. Instead, we find that the cells in Zone 4 endocycle
489 continuously throughout the fly's life, independently of exogenous damage, while at the same
490 time cells are shed into the gut lumen as the fly ages. We find that blocking endocycling in Zone
491 4 causes defects in peritrophic membrane synthesis, and we propose that continual endocycling
492 ensures high levels of peritrophic membrane synthesis throughout the fly's life.
493
494 Endoreplication and polyploidy is extremely widespread in *Drosophila* and across animals and
495 plants, both under healthy, homeostatic conditions and in response to cell or tissue damage

496 [31,53,54,61,62]. In the *Drosophila* larva, many tissues cease mitotic proliferation during
497 embryogenesis, and subsequently grow via developmentally programmed endocycling [31,63].
498 In adult flies, many cell types become polyploid via endoreplication under wildtype conditions,
499 including the nurse cells and follicle cells of the ovary, the enterocytes of the midgut, and rectal
500 papillae cells [61], while other cell types endocycle in response to tissue or cellular damage,
501 including the epidermis in response to wounding [13,62], the hindgut in response to tissue injury
502 [11,12], and the adult brain in response to oxidative and DNA damage [64]. Mammals also
503 display widespread examples of both developmentally programmed endocycling as well as
504 damage-responsive endocycling, including for example in the mammalian liver which displays
505 high levels of endoreplication in response to damage and injury [31,53,54,61,62].
506
507 The pattern of endocycling that we observe in the proventriculus appears to be unique in certain
508 respects compared to other well-characterized examples of endoreplication in *Drosophila* and
509 other tissues. Unlike in the adult brain [64] or ectodermal gut regions including the hindgut
510 [11,12] or the esophagus (Figure 5E), endoreplication in the proventriculus does not occur in
511 response to tissue damage, but is instead reduced by nearby injury (Figure 5). And whereas
512 many other highly metabolically active cells become highly polyploid via endoreplication,
513 including the nurse cells or the follicle cells of the ovary, in those cell types endoreplication
514 appears to proceed for a specific number of cycles and then cease [65], rather than continual
515 endoreplication over the fly's lifespan. What we observe in the proventriculus appears to be a
516 continuous increase in ploidy throughout the adult stage, as part of a homeostatic system that
517 accounts for the steady loss of neighboring cells and also responds to the nutritional input of the
518 fly. We propose that this system may provide insights into how the endocycle can be regulated
519 over long time-scales, as well as into the mechanisms that link age-related cell loss to
520 endoreplication.
521
522 **Methods and Materials**
523
524 **Experimental animals.** Genotypes and sources for *Drosophila melanogaster* lines used in this
525 study are provided in Table S1. Flies were maintained at 18ºC, 25ºC, 29ºC, as indicated in the
526 text, on standard laboratory cornmeal food, except for EdU treatments, yeast supplementation
527 experiments, or drug treatments, which were maintained on Formula 4-24 Instant Blue Food
528 ("Instant Blue Food", Carolina Biological Supply) as described below. All experiments were
529 performed on female flies.
530
531 **EdU feeding and EdU+ cell counting.** EdU (Thermo Fisher) was diluted to 0.2mM in water,
532 then used to hydrate an equal volume of Carolina Instant Blue Food, supplemented with yeast
533 powder as indicated in the text. Adult flies were transferred to EdU-containing food, and flipped
534 to fresh EdU-containing food every two days, for any experiment lasting longer than two days.
535 EdU signal was detected using Click-iT™ EdU Cell Proliferation Kit (Thermo Fisher). Except
536 where noted in the text, 5% yeast was used in EdU experiments (100 mg dried yeast per 2 mL
537 of food), and flies were < 2 weeks old. EdU+ cells were manually counted on a compound
538 epifluorescent microscope, specifically focusing on those EdU+ cells located in Zone 4.
539

540 **Yeast variation experiments.** To test the effect of supplemental dietary yeast on EdU
541 incorporation, dried active yeast was added as a percentage by weight of Instant Blue Food.
542
543 **Colchicine treatment.** To enrich mitotic nuclei, flies were fed with 0.2 mg/mL colchicine (EMD
544 Millipore) for 12 hours prior to dissection. Colchicine was diluted in water and used to dilute
545 Instant Blue Food supplemented with 10% yeast.
546
547 **Gut damage with X-rays, bleomycin, and *ECC15* infection.** For X-ray damage, adult flies
548 were irradiated with 0, 1000, or 2000 RADs in a TORREX 120D X-ray Inspection System
549 (ScanRay Corporation). For gut damage with bleomycin, bleomycin (Sigma) was diluted to 25
550 ng/µL in water and used to rehydrate 2 mL of Instant Blue Food. Flies were fed bleomycin-
551 contained food for two days at 29ºC to increase ingestion, and were flipped to fresh food each
552 day, with water as a control. For *ECC15* treatment, 100mL of LB medium were inoculated with
553 20 µL of a *ECC15* glycerol stock and grown at 30ºC for 20-24 hours. *ECC15* cultures were then
554 centrifuged for 30 minutes at 3000 rpm and resuspended in 1.4 mL of a 5% sucrose. Flies were
555 starved for two hours at 29ºC, and then flipped to a vial containing only a kimwipe soaked in 700
556 µL of the *ECC15* solution, where they fed for 24 hours at 29ºC to induce gut damage. After gut
557 damage, flies were maintained on standard food at 25ºC for the indicated amount of time.
558
559 **Immunohistochemistry and confocal imaging.** Tissues were dissected in 1X phospho-
560 buffered saline (PBS), fixed for 25-30 minutes in 4% paraformaldehyde in PBS, permeabilized in
561 PBS with 0.3% Triton-X (PBST), and stained following standard antibody staining procedures
562 using 5% normal goat serum as a blocking agent. Filamentous actin was stained using Alexa
563 555-coupled phalloidin (Molecular Probes), peritrophic membranes were stained with Alexa647-
564 coupled Lectin HPA (Thermo Fisher), and nuclei were stained using DAPI. Stained tissues were
565 mounted in Vectashield (Vector Labs), except for Alexa647-labeled tissues which were mounted
566 in Prolong Gold (Thermo Fisher Scientific). Rabbit anti-GFP AlexaFluor488 conjugate
567 (Molecular Probes, 1:300) was used to visualize GFP expression, Wg expression was detected
568 using mouse anti-Wg (Developmental Studies Hybridoma Bank 4D4, 1:100) and phospho-
569 Histone 3 was detected using rabbit anti-PH3 (Cell Signaling Technologies 9701S, 1:500).
570 Primary antibodies were detected with Alexa Fluor 488- or 555- coupled secondary antibodies
571 (1:400). Confocal images were captured on a Zeiss LSM 780, LSM 980, or an Olympus IX83
572 confocal microscope, through the Microscopy Resources of the North Quad (MicRoN) facility at
573 Harvard Medical School.
574
575 **Single nucleus RNAseq (snRNAseq) atlas.** To capture proventriculus transcriptional states in
576 both well-fed flies and flies with reduced systemic insulin signaling, single nuclei suspensions
577 were generated from proventriculus samples from both control flies (*esg-Gal4, tubGal80^{ts},*
578 *UAS:GFP /* +) and cachexic flies (*esg-Gal4, tubGal80^{ts}, UAS:GFP ; UAS-yki^{3SA}*), after 8 or 9
579 days at 29ºC. We verified via confocal analysis that *esg-Gal4* is not expressed in the
580 proventriculus itself, which was also confirmed via snRNA sequencing. Proventriculus samples
581 were manually dissected from adult female flies in cold Schneider's medium and immediately
582 flash frozen on dry ice in eppendorf tubes until a total of approximately 600 samples were
583 collected (~300 of each genotype). Proventriculi were manually severed from the crop and

584 esophagus, and from the midgut just posterior to the proventriculus, anterior to where *esg-Gal4*
585 is detected in midgut ISCs.
586
587 Single nuclei were isolated following the protocol described in [66], derived originally from [67],
588 and stained with DAPI immediately before FACS sorting, performed at the Immunology Flow
589 Cytometry Core at Harvard Medical School. Sorted nuclei were resuspended in 1X PBS
590 supplemented with 0.5% BSA with RNAse inhibitor (Promega) at a concentration of ~2000
591 cells/µl.
592
593 snRNAseq was performed following the 10X Genomics Chromium protocol (Chromium Next
594 GEM 551 Single Cell 3'_v3.1_Rev_D), and sequenced using a Illumina NovaSeq 6000 at the
595 Harvard Medical School Biopolymers Facility. 10,525 nuclei from esg^{ts} flies and 11,801 nuclei
596 from esg^{ts} > *yki* flies were sequenced (total = 22,332 nuclei) and reads were mapped to
597 BDGP6.32.
598
599 Bioinformatic analysis was performed largely following [68] with minor modifications. Raw data
600 were processed with Cell Ranger software (10x Genomics, v7.0.0) to generate a single cell
601 matrix for each sample. The count matrices were imported into Seurat (v4.3.0) and cells with
602 less than 1300 or greater than 60,000 UMIs were filtered out, and low abundance genes with
603 less than 10 counts were removed from further analysis. The two biological samples were
604 bioinformatically pooled for PCA and clustering analysis to generate a single atlas including
605 cells from both conditions. After a PCA reduction, the first 40 components were used for UMAP
606 and clustering analysis, at a 0.2 resolution. We removed from further analysis one cluster that
607 appeared to be an artefact, as it contained markers for multiple different unrelated cell-types as
608 well as stress and heat shock proteins. Differentially expressed genes were calculated using the
609 Wilcox Rank Sum Test across each cluster and were then further selected using a Log2FC > X
610 cut-off and adjusted p value < 0.05. All downstream analysis was performed in R (v4.3).
611
612 To map snRNAseq clusters to proventriculus anatomy, we examined the expression pattern of
613 Gal4 lines for top-ranking marker genes using confocal microscopy.
614
615 **MARCM analysis.** Flies of the genotype *hsFLP, FRT19A, tubGal80 ; tub-Gal4, UAS-GFP* were
616 crossed to *FRT19A* flies (BL1709), and offspring were heat-shocked in a 37ºC water bath either
617 during the L3 stage for during the adult stage. Two one hour heat-shocks were administered,
618 separated by 2-3 hours at 25ºC. MARCM crosses were maintained at either 25ºC or 18ºC as
619 indicated in the text.
620
621 **Tissue damage protocol using *UAS-rpr*.** Similarly to [11], we induced ectopic apoptosis by
622 crossing Gal4 drivers to flies containing *UAS-rpr* ; $tubGal80^{ts}$ or, for non-damaged controls, to
623 w^{1118} flies. These crosses were maintained at 18ºC until several days after eclosion. Adult flies
624 were then transferred to EdU+ food and placed at 29ºC for 48 hours to induce apoptosis, then
625 returned to recover at 18ºC for either 2 days or 5 days, on EdU+ food throughout. Thus, all
626 EdU+ incorporation events that occurred during the damage or during the recovery period could
627 be visualized and quantified.

628
629 **Creation of split-intein Gal4 line.** To generate *GMR71F06-Gal4::Gal4-C-int*, the 3,547 bp
630 enhancer fragment from *GMR71F06* FlyLight line [69] was amplified using the following primers:
631 caccTGCCCCGAGCAGCAAAAGAAGTCCG and TCTCCGAAATCTGCGCCAATTCCAG, and
632 cloned into the pENTR-dTOPO vector (Thermo Fisher Scientific). This fragment was cloned into
633 the pBP-Gal4$^{C\text{-}int}$ backbone [39] (Addgene 199202) via LR gateway cloning, and was inserted
634 into the attP40 landing site using standard phiC31 transgenesis.
635
636 **Time series of nuclear morphology.** To quantify nuclear morphology over the course of the
637 fly's life, age matched flies of the genotype *GMR7106-Gal4 / UAS-Stinger ; MKRS /* + were
638 collected on eclosion day, and maintained at 25ºC in standard fly vials on standard lab food
639 (approximately 10-15 adult flies per vial), either with or without dried active yeast sprinkled on
640 the food's surface. In a pilot experiment, we observed that *UAS-Stinger* is tightly nuclear-
641 localized in this tissue, whereas other common nuclear-localized fluorophores transgenes
642 (*UAS:GFP^{NLS}* [BL4776], *UAS-unc84-GFP* [lab stock] and *UAS:RedStinger* [BL8545]) were not.
643 Flies were flipped onto fresh food every two or three days. On each day of sampling (3d, 7d, 14,
644 21d, 28d, and 35d), approximately 6-8 cardia were dissected and stained overnight with Alexa
645 488-coupled anti-GFP, DAPI, and phalloidin as described above. At each time-point, confocal z-
646 stacks were collected through the entirety of Zone 4 (n=5-6 proventriculus per time point) and
647 analyzed as described below. We also collected samples for eclosion day and for 1d later, but
648 found that the Gal4 expression pattern extended beyond Zone 4 at these time points, so they
649 were excluded from further analysis.
650
651 **Image quantification.** Image quantification was performed with arivis Vision4D software (Zeiss,
652 v4.1.2). GFP+ nuclei were segmented using the Cellpose-based Segmenter, and segmentation
653 was then manually corrected for each sample by splitting or removing nuclei which were
654 erroneously fused and removing artefacts that did not correspond to nuclei. Nuclear volume was
655 extracted for all objects >10μm^3. For cell count, those nuclei missed by Cellposed-based
656 segmentation were manually counted using the "add marker" function while viewing the tissue in
657 3D. To quantify cell loss during aging, cells that had been shed into the lumen were manually
658 counted in FIJI [70].
659
660 **Ploidy measurements.** Ploidy was quantified as described in [52]. Flies of the genotype *w ;*
661 *UAS:GFP^{Stinger} ; 71F06-Gal4* were aged to 17-19 days old at 25ºC, and then squashed to a
662 cellular monolayer on a charged slide, in parallel with adult testes samples as a haploid
663 standard. The summed DAPI intensity of GFP+ nuclei were quantified and compared to haploid
664 nuclei measured under the same conditions.
665
666 **Lifespan and *Pseudomonas* survival experiments.** Lifespan experiments were conducted at
667 29ºC, with 15 mated females per vial on standard fly food supplemented with dried yeast
668 powder, and flipped every 1-2 days. Flies of the genotype *w ; tubGal80^{ts} , UAS:GFP ; 71F06-*
669 *Gal4* were crossed to control or UAS:RNAi lines, and the offspring were reared at 18ºC until
670 eclosion. Adults were collected and mated over a 4 day period at 18ºC, then shifted to 29ºC

three days later to begin life-span measurements. The number of dead flies was recorded every day.

Infection with *Pseudomonas aeruginosa (PA14)* followed a protocol similar to [59]. 5mL of LB medium was seeded from a glycerol stock of *PA14* and grown overnight in a shaking 37ºC incubator. The following morning, 1 mL of this culture was diluted in 50 mL of fresh LB and grown for an additional 6 hours, shaking at 37ºC. This culture was then diluted 1:3 in 5% sucrose solution. Fly vials containing half of a standard kimwipe, compressed into the bottom of the vial, were loaded with 1.5 mL of this bacterial suspension. In order to promote feeding on the bacteria, flies were starved for two hours in empty vials immediately prior to bacterial treatment.

These experiments were performed at 29ºC on flies that had been maintained at 29ºC for 15 days prior to *PA14* infection. After a 24 hour infection, flies were flipped to fresh vials containing kimwipes saturated with 5% sucrose solution, and flipped to fresh 5% sucrose solution daily after that. The number of dead flies was recorded approximately every 24 hours. Four vials of 8-10 flies each were used per genotype, and the entire experiment was performed in biological duplicate, with similar results in both experiments.

Graphing and statistical analysis. All graphs were created and statistical tests performed using Prism (GraphPad, v10).

Data Sharing/ Resource Availability

The snRNA-seq Atlas is available for data mining at https://www.flyrnai.org/scRNA/. Raw RNA-seq reads and processed data files have been deposited in the NCBI Gene Expression Omnibus (GEO) database under accession code GSE301009.

Acknowledgements

We thank Mujeeb Qadiri, Austin Veal, and Aram Comjean for assistance with snRNAseq data analysis and sharing, and Rich Binari for assistance with fly work. We thank Hannah Dayton and Liz Lane for reagents and advice with *Pseudomonas* experiments. This work was supported by the National Institute of Health R24 OD031952. NP is an investigator of the Howard Hughes Medical Institute. This article is subject to HHMI's Open Access to Publications policy. HHMI lab heads have previously granted a nonexclusive CC BY 4.0 license to the public and a sublicensable license to HHMI in their research articles. Pursuant to those licenses, the author-accepted manuscript of this article can be made freely available under a CC BY 4.0 license immediately upon publication.

714 **Literature Cited**

715 1. Buchon N, Osman D, David FPA, Fang HY, Boquete J-P, Deplancke B, et al. Morphological
716 and Molecular Characterization of Adult Midgut Compartmentalization in Drosophila. Cell
717 Reports. 2013;3: 1725–1738. doi:10.1016/j.celrep.2013.04.001
718 2. Buchon N, Osman D. All for one and one for all: Regionalization of the Drosophila intestine.
719 Insect Biochem Molec. 2015;67: 2–8. doi:10.1016/j.ibmb.2015.05.015
720 3. Marianes A, Spradling AC. Physiological and stem cell compartmentalization within the
721 Drosophila midgut. Elife. 2013;2: e00886. doi:10.7554/elife.00886
722 4. Ohlstein B, Spradling A. Multipotent Drosophila Intestinal Stem Cells Specify Daughter Cell
723 Fates by Differential Notch Signaling. Science. 2007;315: 988–992.
724 doi:10.1126/science.1136606
725 5. Micchelli CA, Perrimon N. Evidence that stem cells reside in the adult Drosophila midgut
726 epithelium. Nature. 2005;439: 475–479. doi:10.1038/nature04371
727 6. Jiang H, Tian A, Jiang J. Intestinal stem cell response to injury: lessons from Drosophila. Cell
728 Mol Life Sci. 2016;73: 3337–3349. doi:10.1007/s00018-016-2235-9
729 7. Lucchetta EM, Ohlstein B. The Drosophila midgut: a model for stem cell driven tissue
730 regeneration. Wiley Interdiscip Rev: Dev Biol. 2012;1: 781–788. doi:10.1002/wdev.51
731 8. Cheng H, Leblond CP. Origin, differentiation and renewal of the four main epithelial cell types
732 in the mouse small intestine V. Unitarian theory of the origin of the four epithelial cell types. Am
733 J Anat. 1974;141: 537–561. doi:10.1002/aja.1001410407
734 9. Barker N, Es JH van, Kuipers J, Kujala P, Born M van den, Cozijnsen M, et al. Identification
735 of stem cells in small intestine and colon by marker gene Lgr5. Nature. 2007;449: 1003–1007.
736 doi:10.1038/nature06196
737 10. Zwick RK, Ohlstein B, Klein OD. Intestinal renewal across the animal kingdom: comparing
738 stem cell activity in mouse and Drosophila. Am J Physiol-Gastrointest Liver Physiol. 2019;316:
739 G313–G322. doi:10.1152/ajpgi.00353.2018
740 11. Fox DT, Spradling AC. The Drosophila Hindgut Lacks Constitutively Active Adult Stem Cells
741 but Proliferates in Response to Tissue Damage. Cell Stem Cell. 2009;5: 290–297.
742 doi:10.1016/j.stem.2009.06.003
743 12. Cohen E, Allen SR, Sawyer JK, Fox DT. Fizzy-Related dictates A cell cycle switch during
744 organ repair and tissue growth responses in the Drosophila hindgut. eLife. 2018;7: e38327.
745 doi:10.7554/elife.38327
746 13. Losick VP, Fox DT, Spradling AC. Polyploidization and Cell Fusion Contribute to Wound
747 Healing in the Adult Drosophila Epithelium. Curr Biol. 2013;23: 2224–2232.
748 doi:10.1016/j.cub.2013.09.029
749 14. Losick VP, Jun AS, Spradling AC. Wound-Induced Polyploidization: Regulation by Hippo
750 and JNK Signaling and Conservation in Mammals. PLoS ONE. 2016;11: e0151251.
751 doi:10.1371/journal.pone.0151251
752 15. Singh SR, Zeng X, Zheng Z, Hou SX. The adult Drosophila gastric and stomach organs are
753 maintained by a multipotent stem cell pool at the foregut/midgut junction in the cardia
754 (proventriculus). Cell Cycle. 2011;10: 1109–1120. doi:10.4161/cc.10.7.14830
755 16. King DG. Cellular organization and peritrophic membrane formation in the cardia
756 (Proventriculus) of Drosophila melanogaster. J Morphol. 1988;196: 253–282.

757 doi:10.1002/jmor.1051960302
758 17. Wigglesworth VB. The Formation of the Peritrophic Membrane in Insects, with Special
759 Reference to the Larvae of Mosquitoes. J Cell Sci. 1930;s2-73: 593–616. doi:10.1242/jcs.s2-
760 73.292.593
761 18. Rizki MTM. The secretory activity of the proventriculus of Drosophila melanogaster. J Exp
762 Zoöl. 1956;131: 203–221. doi:10.1002/jez.1401310202
763 19. Pankratz MJ, Hoch M. Control of epithelial morphogenesis by cell signaling and integrin
764 molecules in the Drosophila foregut. Development. 1995;121: 1885–1898.
765 doi:10.1242/dev.121.6.1885
766 20. Fuß B, Hoch M. Drosophila endoderm development requires a novel homeobox gene which
767 is a target of Wingless and Dpp signalling. Mech Dev. 1998;79: 83–97. doi:10.1016/s0925-
768 4773(98)00172-5
769 21. Fuss B, Josten F, Feix M, Hoch M. Cell movements controlled by the Notch signalling
770 cascade during foregut development in Drosophila. Development. 2004;131: 1587–1595.
771 doi:10.1242/dev.01057
772 22. Waterhouse D. The Rate of Production of the Peritrophic Membrane in Some Insects. Aust
773 J Biol Sci. 1954;7: 59–72. doi:10.1071/bi9540059
774 23. Becker B. Determination of the formation rate of peritrophic membranes in some Diptera. J
775 Insect Physiol. 1978;24: 529–533. doi:10.1016/0022-1910(78)90054-9
776 24. Tzou P, Ohresser S, Ferrandon D, Capovilla M, Reichhart J-M, Lemaitre B, et al. Tissue-
777 Specific Inducible Expression of Antimicrobial Peptide Genes in Drosophila Surface Epithelia.
778 Immunity. 2000;13: 737–748. doi:10.1016/s1074-7613(00)00072-8
779 25. Zhu H, Ludington WB, Spradling AC. Cellular and molecular organization of the Drosophila
780 foregut. Proc Natl Acad Sci. 2024;121: e2318760121. doi:10.1073/pnas.2318760121
781 26. Dodge R, Jones EW, Zhu H, Obadia B, Martinez DJ, Wang C, et al. A symbiotic physical
782 niche in Drosophila melanogaster regulates stable association of a multi-species gut microbiota.
783 Nat Commun. 2023;14: 1557. doi:10.1038/s41467-023-36942-x
784 27. Bertran-Mas J, Giorgio ED, Martín N, Llimargas M. Different cellular and molecular
785 mechanisms of chitin deposition contribute to the specificity of the two chitin synthases in D.
786 melanogaster. bioRxiv. 2024; 2024.12.02.626067. doi:10.1101/2024.12.02.626067
787 28. Pandey A, Galeone A, Han SY, Story BA, Consonni G, Mueller WF, et al. Gut barrier
788 defects, intestinal immune hyperactivation and enhanced lipid catabolism drive lethality in
789 NGLY1-deficient Drosophila. Nat Commun. 2023;14: 5667. doi:10.1038/s41467-023-40910-w
790 29. Zhang L, Turner B, Ribbeck K, Hagen KGT. Loss of the mucosal barrier alters the
791 progenitor cell niche via Janus kinase/signal transducer and activator of transcription
792 (JAK/STAT) signaling. J Biol Chem. 2017;292: 21231–21242. doi:10.1074/jbc.m117.809848
793 30. Britton JS, Edgar BA. Environmental control of the cell cycle in Drosophila: nutrition
794 activates mitotic and endoreplicative cells by distinct mechanisms. Development. 1998;125:
795 2149–2158. doi:10.1242/dev.125.11.2149
796 31. Edgar BA, Orr-Weaver TL. Endoreplication Cell Cycles More for Less. Cell. 2001;105: 297–
797 306. doi:10.1016/s0092-8674(01)00334-8
798 32. Kwon Y, Song W, Droujinine IA, Hu Y, Asara JM, Perrimon N. Systemic Organ Wasting
799 Induced by Localized Expression of the Secreted Insulin/IGF Antagonist ImpL2. Dev Cell.
800 2015;33: 36–46. doi:10.1016/j.devcel.2015.02.012

801 33. Ding G, Xiang X, Hu Y, Xiao G, Chen Y, Binari R, et al. Coordination of tumor growth and
802 host wasting by tumor-derived Upd3. Cell Rep. 2021;36: 109553.
803 doi:10.1016/j.celrep.2021.109553
804 34. Liu Y, Saavedra P, Perrimon N. Cancer cachexia: lessons from Drosophila. Dis Model
805 Mech. 2022;15: dmm049298. doi:10.1242/dmm.049298
806 35. Lim SY, You H, Lee J, Lee J, Lee Y, Lee K-A, et al. Identification and characterization of
807 GAL4 drivers that mark distinct cell types and regions in the Drosophila adult gut. J Neurogenet.
808 2021;35: 33–44. doi:10.1080/01677063.2020.1853722
809 36. Ghosh S, Leng W, Wilsch-Bräuninger M, Barrera-Velázquez M, Léopold P, Eaton S. A local
810 insulin reservoir in Drosophila alpha cell homologs ensures developmental progression under
811 nutrient shortage. Curr Biol. 2022;32: 1788-1797.e5. doi:10.1016/j.cub.2022.02.068
812 37. Kim SK, Rulifson EJ. Conserved mechanisms of glucose sensing and regulation by
813 Drosophila corpora cardiaca cells. Nature. 2004;431: 316–320. doi:10.1038/nature02897
814 38. Lee G, Park JH. Hemolymph Sugar Homeostasis and Starvation-Induced Hyperactivity
815 Affected by Genetic Manipulations of the Adipokinetic Hormone-Encoding Gene in Drosophila
816 melanogaster. Genetics. 2004;167: 311–323. doi:10.1534/genetics.167.1.311
817 39. Ewen-Campen B, Luan H, Xu J, Singh R, Joshi N, Thakkar T, et al. split-intein Gal4
818 provides intersectional genetic labeling that is repressible by Gal80. Proc Natl Acad Sci United
819 States Am. 2023;120: e2304730120. doi:10.1073/pnas.2304730120
820 40. Hung R-J, Hu Y, Kirchner R, Liu Y, Xu C, Comjean A, et al. A cell atlas of the adult
821 Drosophila midgut. Proc National Acad Sci. 2020;117: 1514–1523.
822 doi:10.1073/pnas.1916820117
823 41. Ren F, Wang B, Yue T, Yun E-Y, Ip YT, Jiang J. Hippo signaling regulates Drosophila
824 intestine stem cell proliferation through multiple pathways. Proc National Acad Sci. 2010;107:
825 21064–21069. doi:10.1073/pnas.1012759107
826 42. Karpowicz P, Perez J, Perrimon N. The Hippo tumor suppressor pathway regulates
827 intestinal stem cell regeneration. Development (Cambridge, England). 2010;137: 4135–4145.
828 doi:10.1242/dev.060483
829 43. Shaw RL, Kohlmaier A, Polesello C, Veelken C, Edgar BA, Tapon N. The Hippo pathway
830 regulates intestinal stem cell proliferation during Drosophila adult midgut regeneration.
831 Development. 2010;137: 4147–4158. doi:10.1242/dev.052506
832 44. Jiang H, Grenley MO, Bravo M-J, Blumhagen RZ, Edgar BA. EGFR/Ras/MAPK Signaling
833 Mediates Adult Midgut Epithelial Homeostasis and Regeneration in Drosophila. Cell Stem Cell.
834 2011;8: 84–95. doi:10.1016/j.stem.2010.11.026
835 45. Xu C, Luo J, He L, Montell C, Perrimon N. Oxidative stress induces stem cell proliferation
836 via TRPA1/RyR-mediated Ca2+ signaling in the Drosophila midgut. eLife. 2017;6: e22441.
837 doi:10.7554/elife.22441
838 46. Leung NY, Xu C, Li JSS, Ganguly A, Meyerhof GT, Regimbald-Dumas Y, et al. Gut tumors
839 in flies alter the taste valence of an anti-tumorigenic bitter compound. Curr Biol. 2024;34: 2623-
840 2632.e5. doi:10.1016/j.cub.2024.04.082
841 47. Ohlstein B, Spradling A. The adult Drosophila posterior midgut is maintained by pluripotent
842 stem cells. Nature. 2006;439: 470–474. doi:10.1038/nature04333
843 48. McLeod CJ, Wang L, Wong C, Jones DL. Stem cell dynamics in response to nutrient
844 availability. Current biology : CB. 2010;20: 2100–2105. doi:10.1016/j.cub.2010.10.038

845 49. Lucchetta EM, Ohlstein B. Amitosis of Polyploid Cells Regenerates Functional Stem Cells
846 in the Drosophila Intestine. Stem Cell. 2017;20: 1–19. doi:10.1016/j.stem.2017.02.012
847 50. Miguel-Aliaga I, Jasper H, Lemaitre B. Anatomy and Physiology of the Digestive Tract of
848 Drosophila melanogaster. Genetics. 2018;210: 357–396. doi:10.1534/genetics.118.300224
849 51. Evans CJ, Olson JM, Ngo KT, Kim E, Lee NE, Kuoy E, et al. G-TRACE: rapid Gal4-based
850 cell lineage analysis in Drosophila. Nat Methods. 2009;6: 603–5. doi:10.1038/nmeth.1356
851 52. Clay DE, Stormo BM, Fox DT. Measuring Cellular Ploidy In Situ by Light Microscopy.
852 Methods Mol Biol (Clifton, NJ). 2023;2545: 401–412. doi:10.1007/978-1-0716-2561-3_21
853 53. Morris JP, Baslan T, Soltis DE, Soltis PS, Fox DT. Integrating the Study of Polyploidy
854 Across Organisms, Tissues, and Disease. Annu Rev Genet. 2024. doi:10.1146/annurev-genet-
855 111523-102124
856 54. Øvrebø JI, Edgar BA. Polyploidy in tissue homeostasis and regeneration. Development.
857 2018;145: dev156034. doi:10.1242/dev.156034
858 55. Molano-Fernández M, Hickson ID, Herranz H. Cyclin E overexpression in the Drosophila
859 accessory gland induces tissue dysplasia. Front Cell Dev Biol. 2023;10: 992253.
860 doi:10.3389/fcell.2022.992253
861 56. Pierce SB, Yost C, Britton JS, Loo LWM, Flynn EM, Edgar BA, et al. dMyc is required for
862 larval growth and endoreplication in Drosophila. Development. 2004;131: 2317–2327.
863 doi:10.1242/dev.01108
864 57. Demontis F, Perrimon N. Integration of Insulin receptor/Foxo signaling and dMyc activity
865 during muscle growth regulates body size in Drosophila. Development (Cambridge, England).
866 2009;136: 983–993. doi:10.1242/dev.027466
867 58. Kuraishi T, Binggeli O, Opota O, Buchon N, Lemaitre B. Genetic evidence for a protective
868 role of the peritrophic matrix against intestinal bacterial infection in Drosophila melanogaster.
869 Proc Natl Acad Sci. 2011;108: 15966–15971. doi:10.1073/pnas.1105994108
870 59. Kim K, Hung R-J, Perrimon N. miR-263a Regulates ENaC to Maintain Osmotic and
871 Intestinal Stem Cell Homeostasis in Drosophila. Dev Cell. 2017;40: 23–36.
872 doi:10.1016/j.devcel.2016.11.023
873 60. Kim K, Lane EA, Saftien A, Wang H, Xu Y, Wirtz-Peitz F, et al. Drosophila as a model for
874 studying cystic fibrosis pathophysiology of the gastrointestinal system. Proc Natl Acad Sci.
875 2020;117: 10357–10367. doi:10.1073/pnas.1913127117
876 61. Fox DT, Duronio RJ. Endoreplication and polyploidy: insights into development and
877 disease. Development. 2012;140: 3–12. doi:10.1242/dev.080531
878 62. Bailey EC, Kobielski S, Park J, Losick VP. Polyploidy in Tissue Repair and Regeneration.
879 Cold Spring Harb Perspect Biol. 2021;13: a040881. doi:10.1101/cshperspect.a040881
880 63. Smith AV, Orr-Weaver TL. The regulation of the cell cycle during Drosophila
881 embryogenesis: the transition to polyteny. Development. 1991;112: 997–1008.
882 doi:10.1242/dev.112.4.997
883 64. Nandakumar S, Grushko O, Buttitta LA. Polyploidy in the adult Drosophila brain. eLife.
884 2020;9: e54385. doi:10.7554/elife.54385
885 65. Zielke N, Edgar BA, DePamphilis ML. Endoreplication. Cold Spring Harb Perspect Biol.
886 2013;5: a012948. doi:10.1101/cshperspect.a012948
887 66. Liu Y, Dantas E, Ferrer M, Liu Y, Comjean A, Davidson EE, et al. Tumor Cytokine-Induced
888 Hepatic Gluconeogenesis Contributes to Cancer Cachexia: Insights from Full Body Single

889 Nuclei Sequencing. bioRxiv. 2023; 2023.05.15.540823. doi:10.1101/2023.05.15.540823
890 67. Li H, Janssens J, Waegeneer MD, Kolluru SS, Davie K, Gardeux V, et al. Fly Cell Atlas: A
891 single-nucleus transcriptomic atlas of the adult fruit fly. Science. 2022;375: eabk2432.
892 doi:10.1126/science.abk2432
893 68. Saavedra P, Dumesic PA, Hu Y, Filine E, Jouandin P, Binari R, et al. REPTOR and
894 CREBRF encode key regulators of muscle energy metabolism. Nat Commun. 2023;14: 4943.
895 doi:10.1038/s41467-023-40595-1
896 69. Jenett A, Rubin GM, Ngo T-TB, Shepherd D, Murphy C, Dionne H, et al. A GAL4-Driver
897 Line Resource for Drosophila Neurobiology. Cell Reports. 2012;2: 991–1001.
898 doi:10.1016/j.celrep.2012.09.011
899 70. Schindelin J, Arganda-Carreras I, Frise E, Kaynig V, Longair M, Pietzsch T, et al. Fiji: an
900 open-source platform for biological-image analysis. Nat Methods. 2012;9: 676–682.
901 doi:10.1038/nmeth.2019

902

903

Main Figures

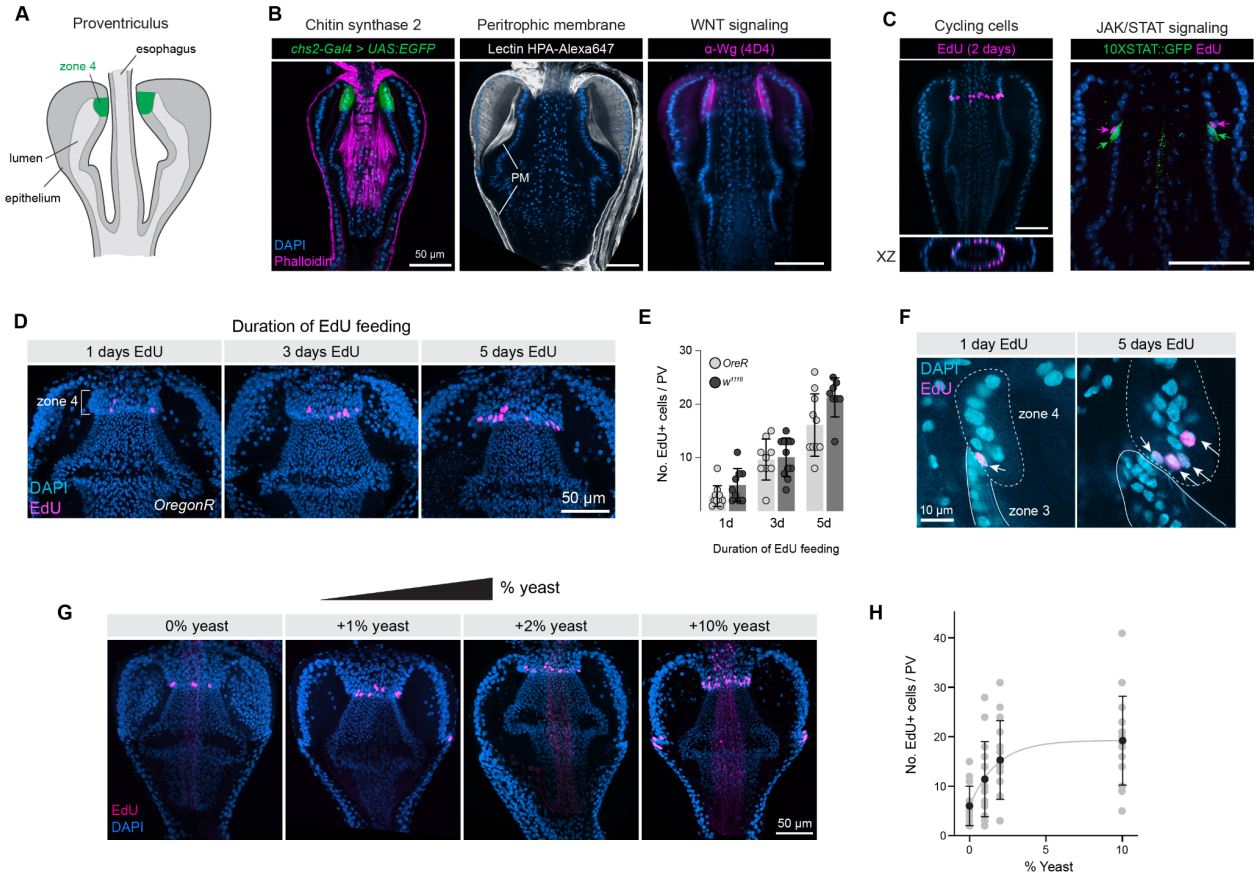

Figure 1. The *Drosophila* proventriculus contains a ring of nutrition-sensitive EdU+ cells located in Zone 4. (A) Schematic of the single-cell epithelium comprising the *Drosophila* proventriculus, located at the juncture of the foregut and anterior midgut. Zone 4 cells are indicated in green. (B) Left panel: *chitin synthase 2* (*Chs2-Gal4*) is specifically expressed in Zone 4 cells. Middle panel: HPA lectin stains the peritrophic membrane (PM). Left panel: Wg protein is enriched in Zone 4 cells. Confocal z-slices are shown. (C) Left panel: EdU labeling is enriched in a ring of cells at the posterior edge of Zone 4. A maximum intensity projection of EdU staining is overlaid on a single z-slice of DAPI staining. Right panel: EdU+ cells are immediately anterior to a ring of cells expressing the 10XSTAT:GFP reporter. Single z-slice is shown. Scale bar is 50 µm. (D) The number of EdU+ cells increases with the duration of EdU feeding. Maximum intensity projections are shown. (E) Quantification of EdU+ cell numbers at 1, 3, and 5 days of feeding, for two different fly strains, *OregonR* and w^{1118}. (F) After a 1 day EdU pulse, staining is largely restricted to small nuclei at the border of Zone 3 and Zone 4. After 5 days of EdU feeding, staining is also visible in larger nuclei. Confocal z-slices are shown. (G) The number of EdU+ cells increases as more yeast is added to the food source. Maximum intensity projections are shown. (H) Quantification of the experiment shown in (G). Anterior is up.

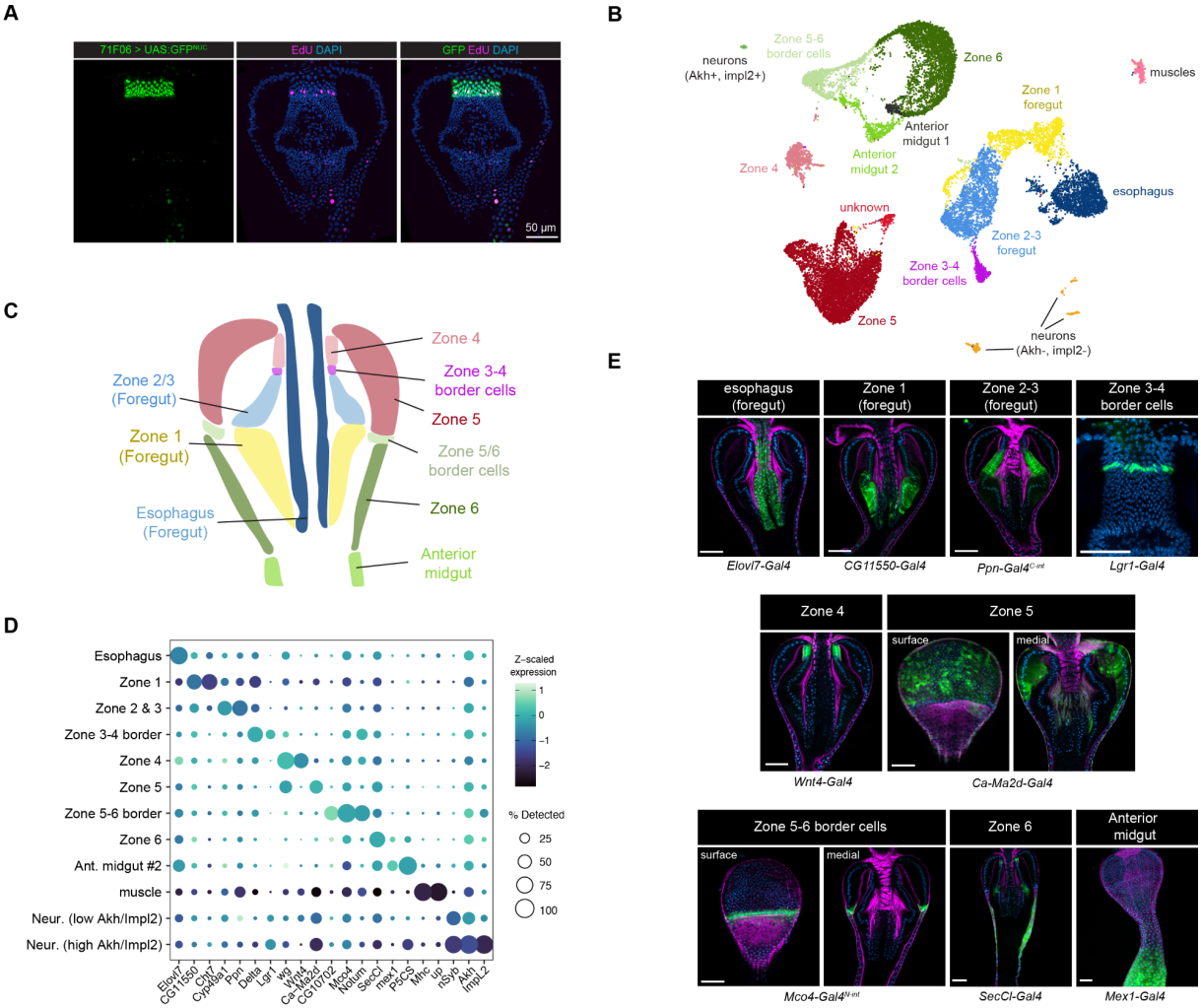

Figure 2. Molecular markers and a single-nuclei atlas for the proventriculus. (A) 71F06-Gal4 drives specific expression in Zone 4 cells, including EdU+ cells. (B) UMAP projection of a single snRNAseq dataset created from 22,332 nuclei, containing 14 clusters representing the major epithelial, muscle, and neuronal cells found in the proventriculus. (C) Schematic of the major epithelial cell types in the proventriculus, corresponding to the clusters identified in (B). (D) Dot plot of selected marker genes for the 12 major clusters identified via snRNAseq; note that two minor clusters ("anterior midgut 1" and "unknown") are excluded from this figure as they could not be clearly linked to *in vivo* cell types. (E) Expression patterns of marker genes for each of the 9 major epithelial cell types in the proventriculus. Anterior is up. Confocal z-slices are shown.

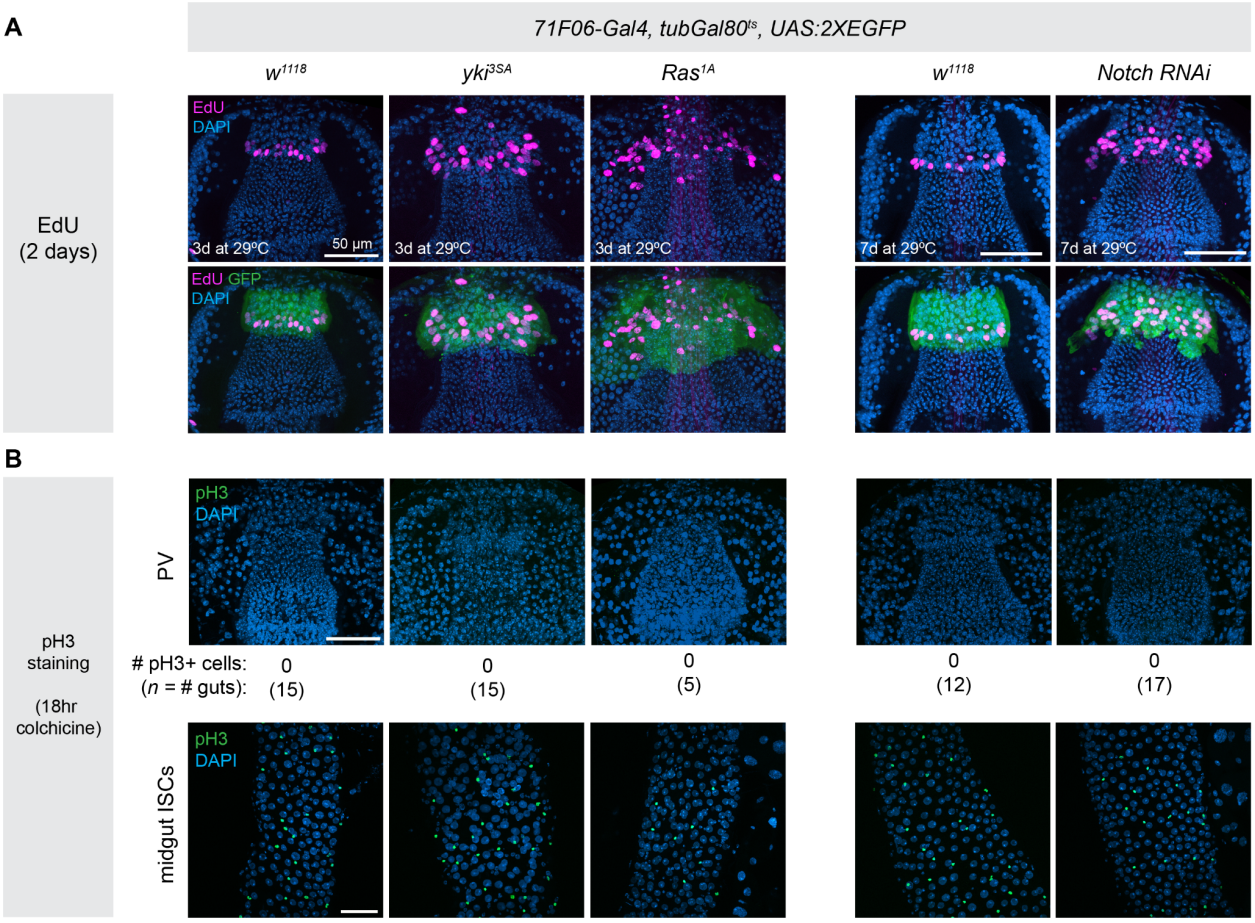

Figure 3. Mitosis is undetectable in Zone 4 cells. (A) Over-expression of the tumor drivers *yki*^{3SA}, *Ras*^{1A}, or *Notch* RNAi in Zone 4 cells causes increased EdU+ incorporation and enlarged and altered morphology of the tissue. (B) No phospho-histone 3 staining was detected in any of the proventriculi examined in any of these genotypes. Flies were fed colchecine for 18 hours prior to dissection to enrich for pH3+ cells. Midgut ISCs from these same guts were included as positive controls, which contained high numbers of pH3+ staining in all samples. Maximum intensity projections are shown. Anterior is up.

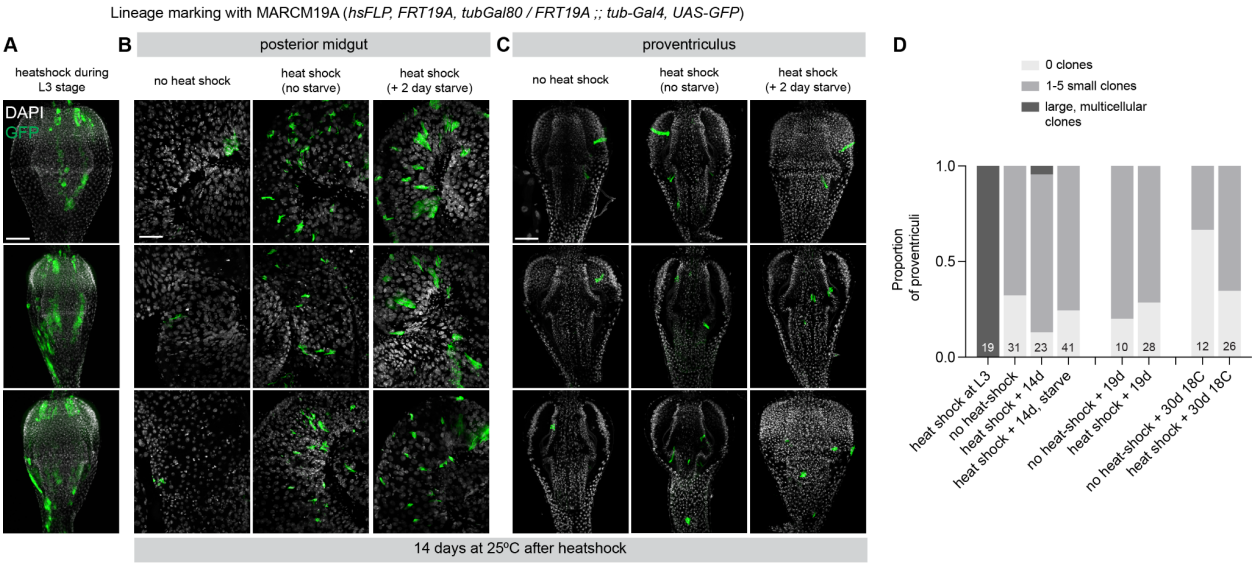

Figure 4. Clonal analysis with MARCM does not label large clones in Zone 4. (A) Positive control for clone induction; clones were induced during the L3 larval stage, leading to large GFP+ clones throughout the proventriculus including in Zone 4. (B) In the posterior midgut, clone induction labels ISCs their descendants and generates GFP+ clones throughout the midgut. These clones are generally larger when flies endure a 2-day starvation followed by re-feeding. (C) In the proventriculus, small scattered GFP+ cells are detected throughout the tissue, but no discernable enrichment in Zone 4, where EdU+ cells are located. (D) Quantification of several MARCM experiments, with dissection 14 days after clone induction (at 25ºC), 19 days after clone induction (at 25ºC), or 30days after clone induction (at 18ºC). Maximum intensity projections are shown. Scale bar = 50μm. Anterior is up.

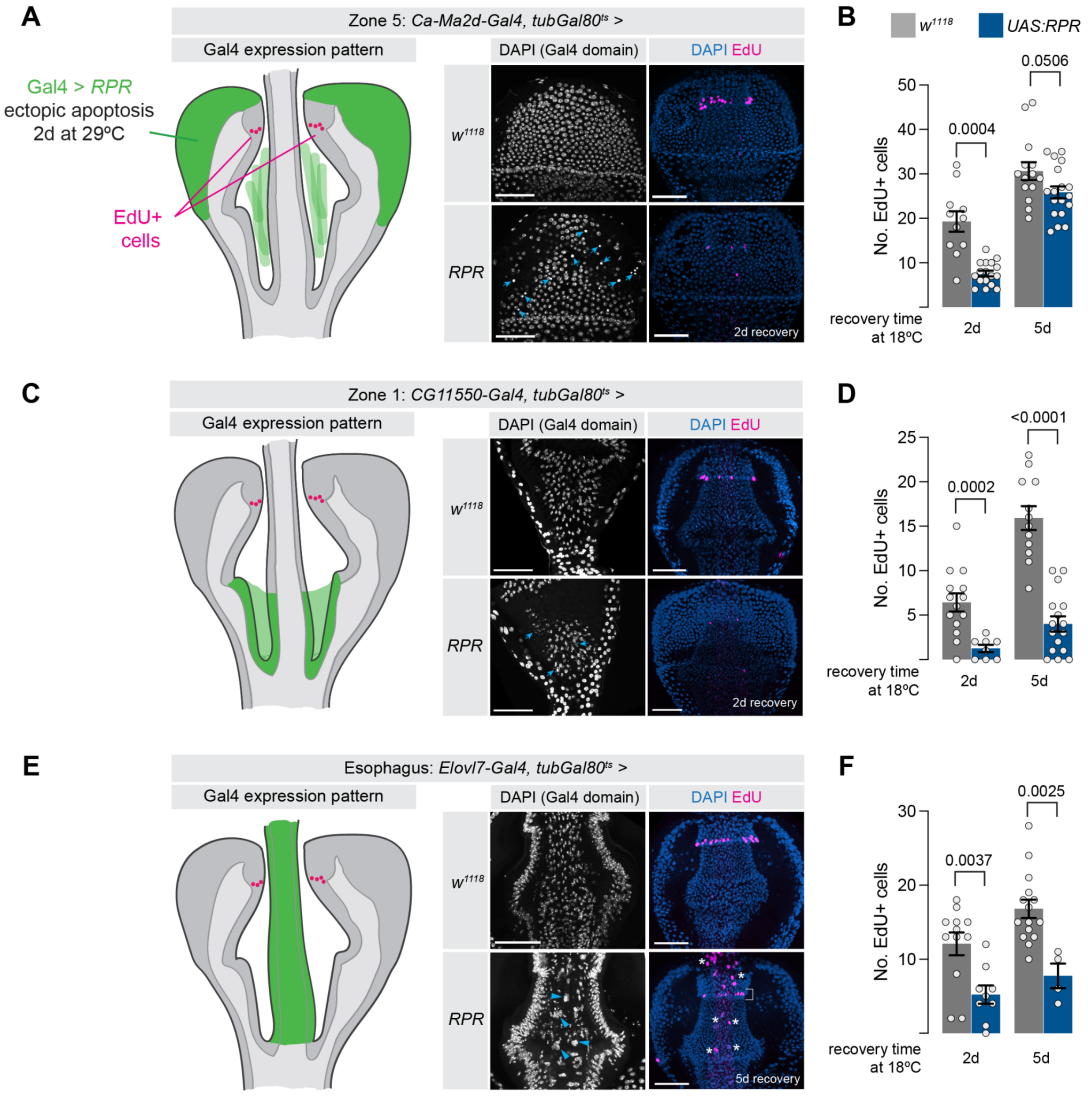

Figure 5. Tissue damage causes a decrease, not an increase, in Zone 4 cell cycling. Tissue damage was induced by over-expressing the pro-apoptotic gene *rpr* for two days, in 3 distinct cell types of the proventriculus, and EdU+ cells were visualized after two and five days of recovery. (A) *rpr* expression in Zone 5, using *Ca-Ma2d-Gal4*, causes a decrease in EdU+ cells after both two and five days. Blue arrows indicate pyknotic nuclei indicative of cell death. (B) Quantification of experiment shown in (A). (C) *rpr* expression in Zone 1, using *CG11550-Gal4,* causes a decrease in EdU+ cells after both two and five days. (D) Quantification of experiment shown in (C). (E) *rpr* expression in the esophagus, using *ELOVL7-Gal4*, leads to decreased EdU+ cells in Zone 4, and endoreplication in esophageal cells. White bracket indicates EdU+ signal in Zone 4, blue arrowheads and white asterisks indicate large, EdU+ nuclei in the esophagus itself. Scale bar = 50µm. Anterior is up. (F) Quantification of experiment shown in E. Significance values are from t-test, with Welch's correction for any comparisons with unequal variances.

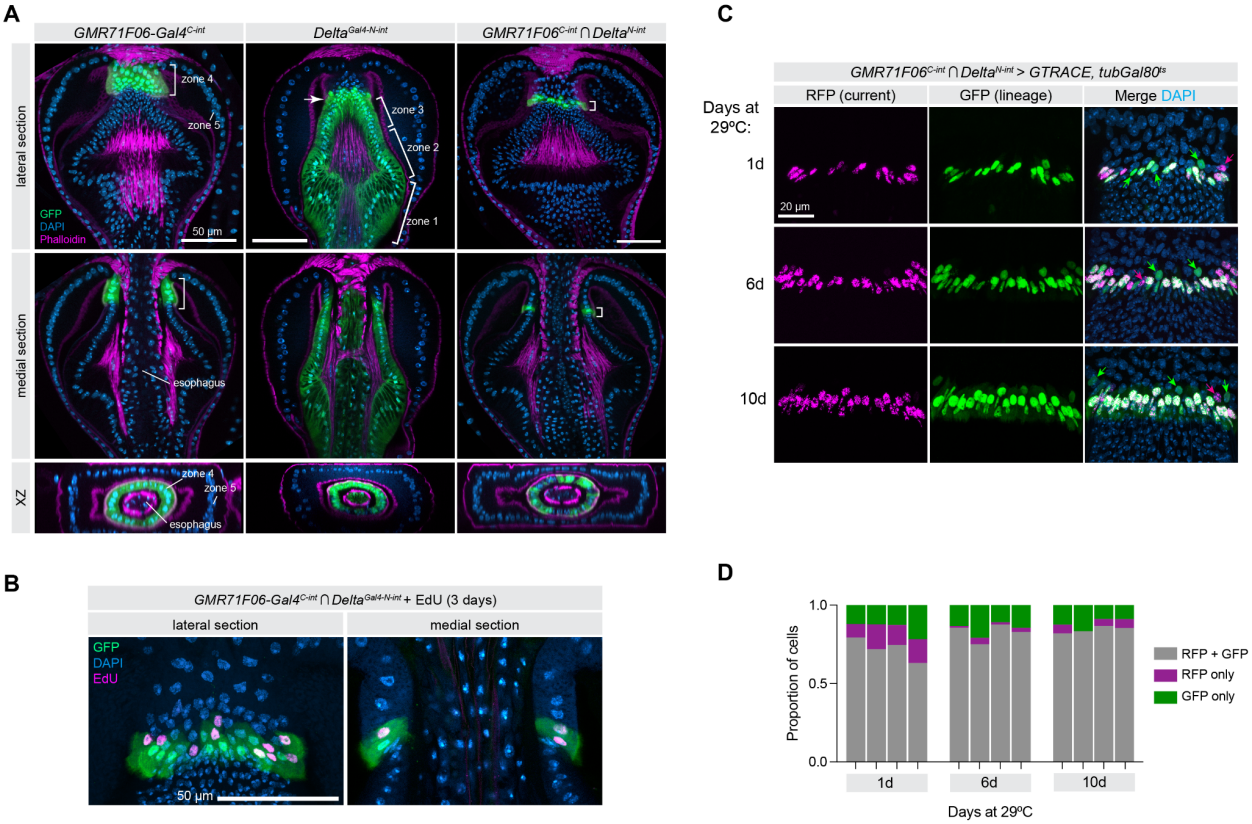

Figure 6. Genetic lineage tracing using a highly-specific split-intein Gal4 that labels Edu+ cells. (A) Expression pattern of *71F06-Gal4::Gal4-C-int*, *Delta*$^{Gal4\text{-}N\text{-}int}$, and the intersection of *71F06 ∩ Delta*. (B) *71F06 ∩ Delta* expression largely overlaps with EdU+ cells in Zone 4 cells. (C) Using *71F06 ∩ Delta* to drive the G-TRACE lineage system, with *tubGal80*^{ts} to restrict labeling to the adult stage for the indicated duration. Colored arrows indicate individual cells with either solely GFP (past but not current expression) or RFP (very recently initiated expression.) Anterior is up.(D) Quantification of experiment shown in (C). Each column represents a single proventriculus sample at the indicated time-point.

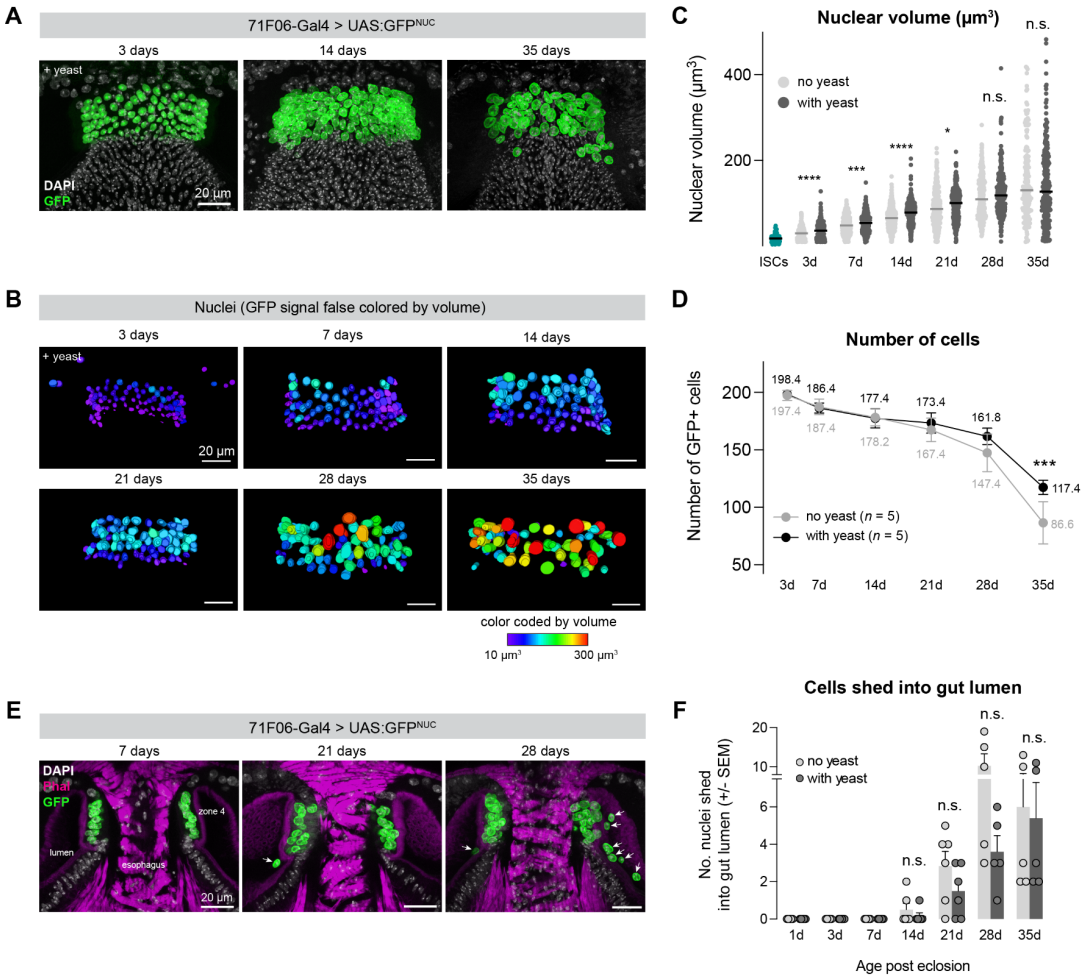

Figure 7. Zone 4 nuclear volume progressively increases over the fly lifespan, while some cells are shed into the gut lumen during aging. (A) Time-course of nuclear morphology of the lifespan of the fly, from three days to 35 days post-eclosion. Nuclear-localized GFP (UAS:GFP^{Stinger}) was expressed in Zone 4 using 71F06-Gal4, and flies were provided with or without supplemental yeast powder. (B) Nuclei were false-colored by volume, indicating a consistent increase in nuclear volume over the course of a fly's life. A posterior-to-anterior gradient of increasingly large nuclear volume is also apparent. (C) Quantification of nuclear volume of Zone 4 nuclei, as well as diploid ISCs for comparison. Nuclear volume increases throughout the lifespan of a fly, with consistently higher volumes for yeast-supplemented flies until the 35d timepoint. "n.s." = not significantly different; * $p = 0.02$; *** $p = 0.0005$; **** $p < 0.0001$, t-test, with Welch's correction for any comparison with unequal variances. (D) The number of Zone 4 cells steadily decreases throughout this time-course, and decreases faster in the absence of yeast powder. *** $p = 0.007$, t-test. (E) GFP+ nuclei are consistently observed shed into the lumen adjacent to Zone 4. (F) Quantification of GFP+ cells observed in the lumen at each time point.

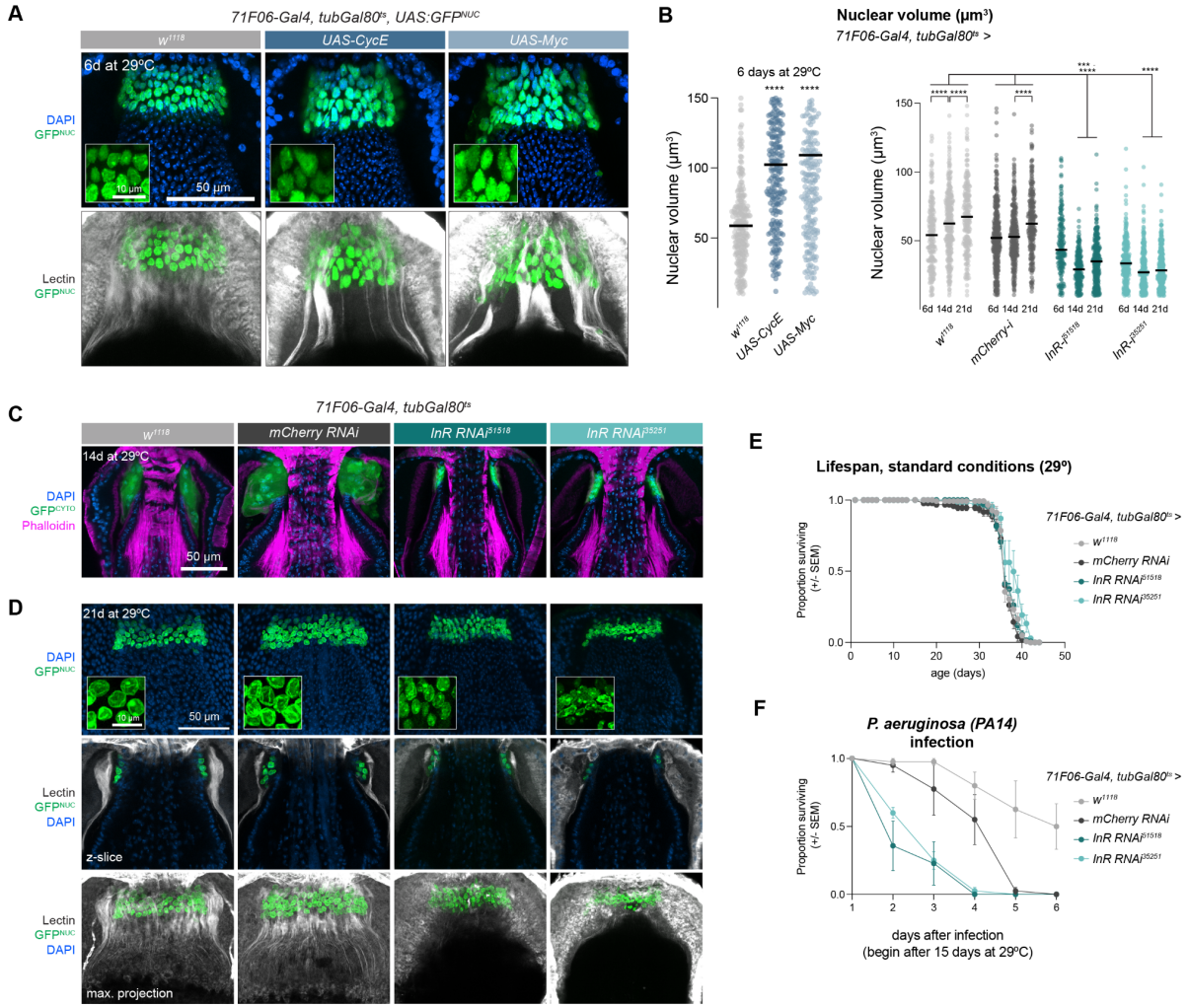

Figure 8. Perturbations to endocycling in Zone 4 cells lead to altered nuclear volume, tissue size, and peritrophic membrane synthesis. (A) Ectopic expression of CycE or Myc drives excess endocycling, leading to larger nuclei (top) and increased peritrophic membrane synthesis from Zone 4 cells, visualized with HPA-lectin. Insets show increased magnification of nuclear GFP. Images are maximum intensity projections of confocal z-stacks (B) Quantification of nuclear volume of *UAS:CycE, UAS:Myc* (n = 4 proventriculi per genotype, 231-255 nuclei per genotype), and *InR RNAi* experiments (n = 3-5 proventriculi, 179-346 nuclei per genotype per timepoint). Statistical tests are one-way ANOVA with multiple comparisons; *** $p < 0.001$; **** $p < 0.0001$. (C) Cytoplasmic UAS:EGFP expression reveals that RNAi against *InR* reduces the overall size of Zone 4. Images are single confocal z-slices. (D) The peritrophic membrane, stained with HPA-Lectin, is reduced and disrupted when endocycling is blocked by RNAi against *InR.* Top two row shows maximum intensity projection, middle row shows single z-stack, and bottom row shows maximum intensity projection.(E) Lifespan at 29ºC under standard conditions is not affected by *InR RNAi*. Sample sizes: *w* = 134; *mCherry RNAi* = 95 flies; *InR RNAi 51518* = 128 flies; *InR RNAi 35251* = 58 flies; 15 flies per vial in all cases. (F) RNAi against *InR* in Zone 4 leads to increased susceptibility to *P. aeruginosa* infection. Sample sizes: *w* = 40 flies;

mCherry RNAi = 40 flies; *InR RNAi 51518* = 38 flies; *InR RNAi 35251* = 40 flies; 9-10 flies per vial.

Supplemental Figures

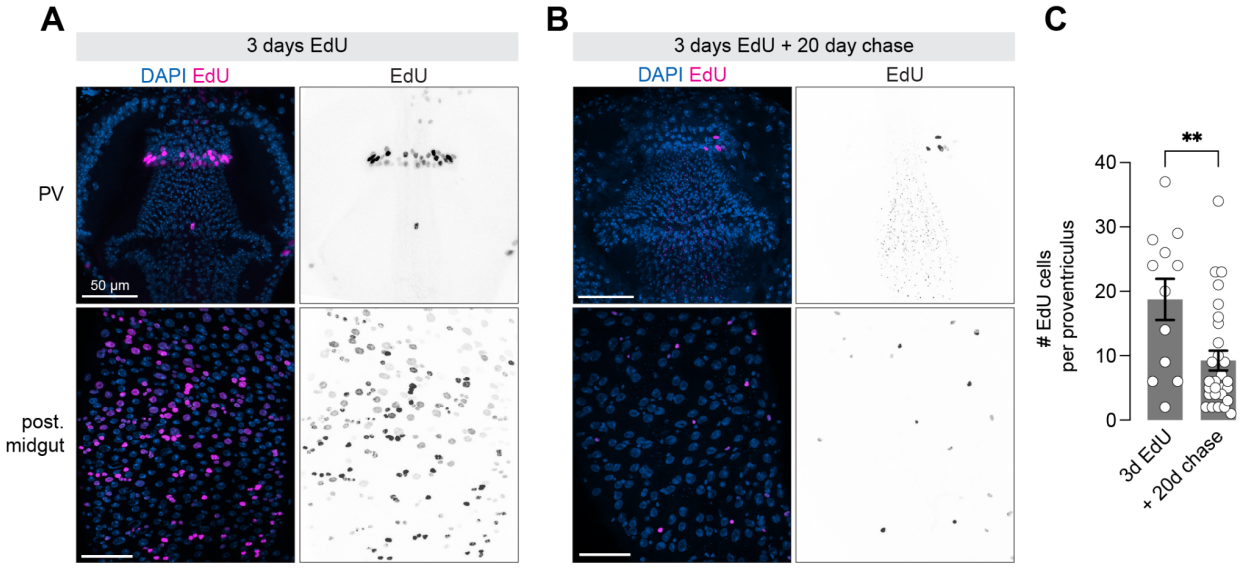

Supplemental Figure 1. EdU+ cells continue cycling throughout adult life. (A) After 3 days of EdU feeding, a ring of labeled cells is visible at the posterior edge of Zone 4, as well as in the ISCs and enterocytes of the midgut. (B) Following a 20 day chase period, a reduction of EdU+ cells is visible in both Zone 4 cells and in the midgut, where continual cycling has diluted out the original EdU pulse.

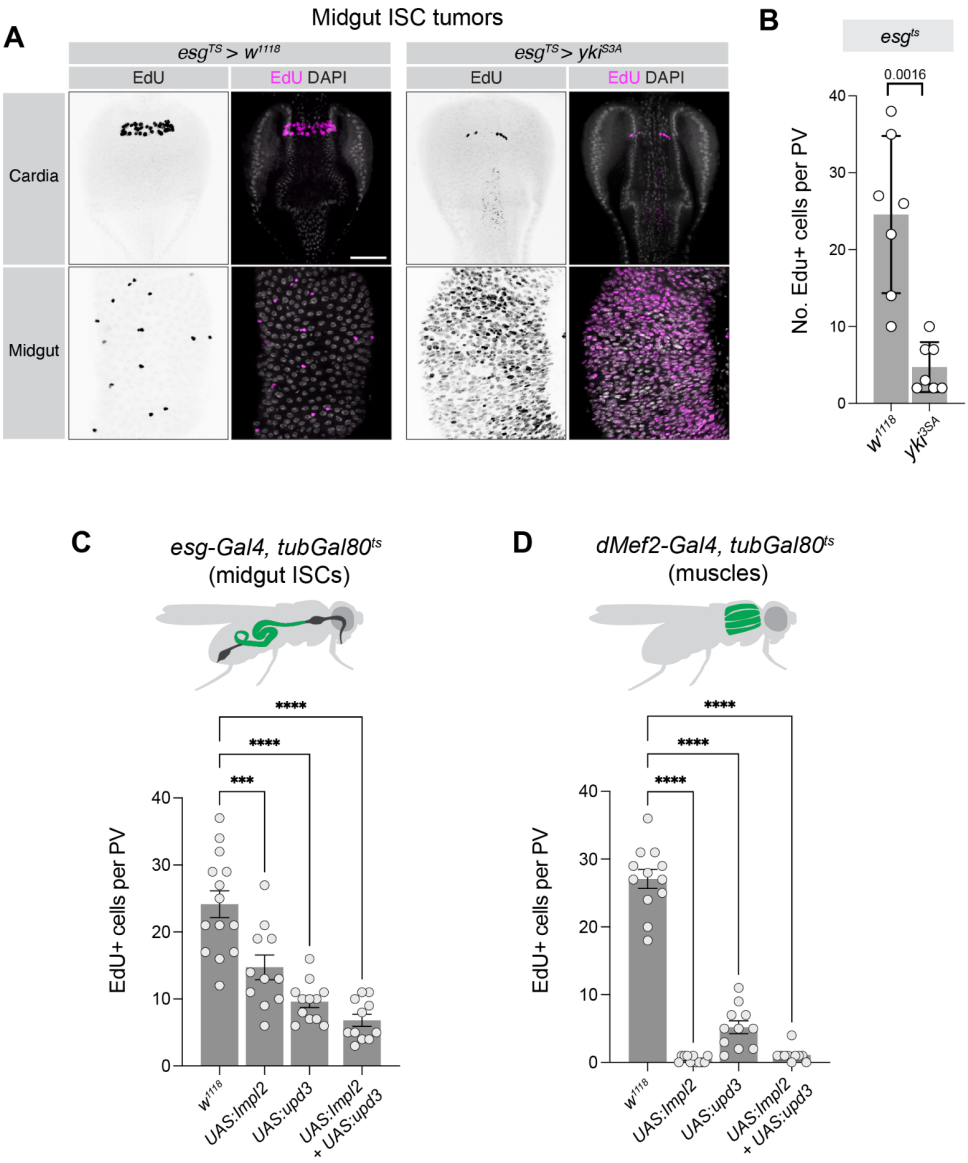

Supplemental Figure 2. Systemic reduction in insulin signaling reduces the number of EdU+ cells in the proventriculus. (A) Tumors in midgut ISCs (driven by *esg-Gal4* > *yki*^{3SA}) cause a reduction in EdU+ cells in the proventriculus. Note that *esg-Gal4* is not expressed in the proventriculus. Anterior is up, scale bar is 50 µm. (B) Quantification of the experiment shown in (A). (C) Over-expression of insulin-antagonists *ImpL2, upd3,* or a combination of both from the ISCs (*esg-Gal4*) leads to a reduction in EdU+ cells. (D) Over-expression of insulin-antagonists *ImpL2, upd3,* or a combination of both from muscles using *dMef2-Gal4* leads to a reduction in EdU+ cells.

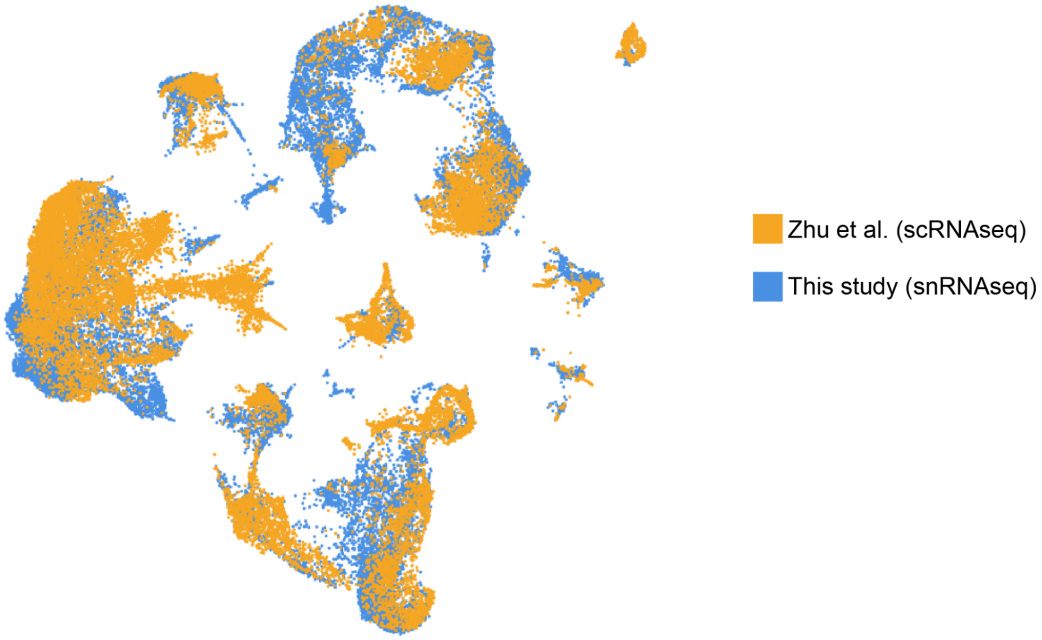

Supplemental Figure 3. Merged UMAP projection of two single cell atlases of the proventriculus. Data from the snRNAseq atlas presented in this manuscript and scRNAseq data from [25] were bioinformatically pooled and re-analyzed into a single dataset.

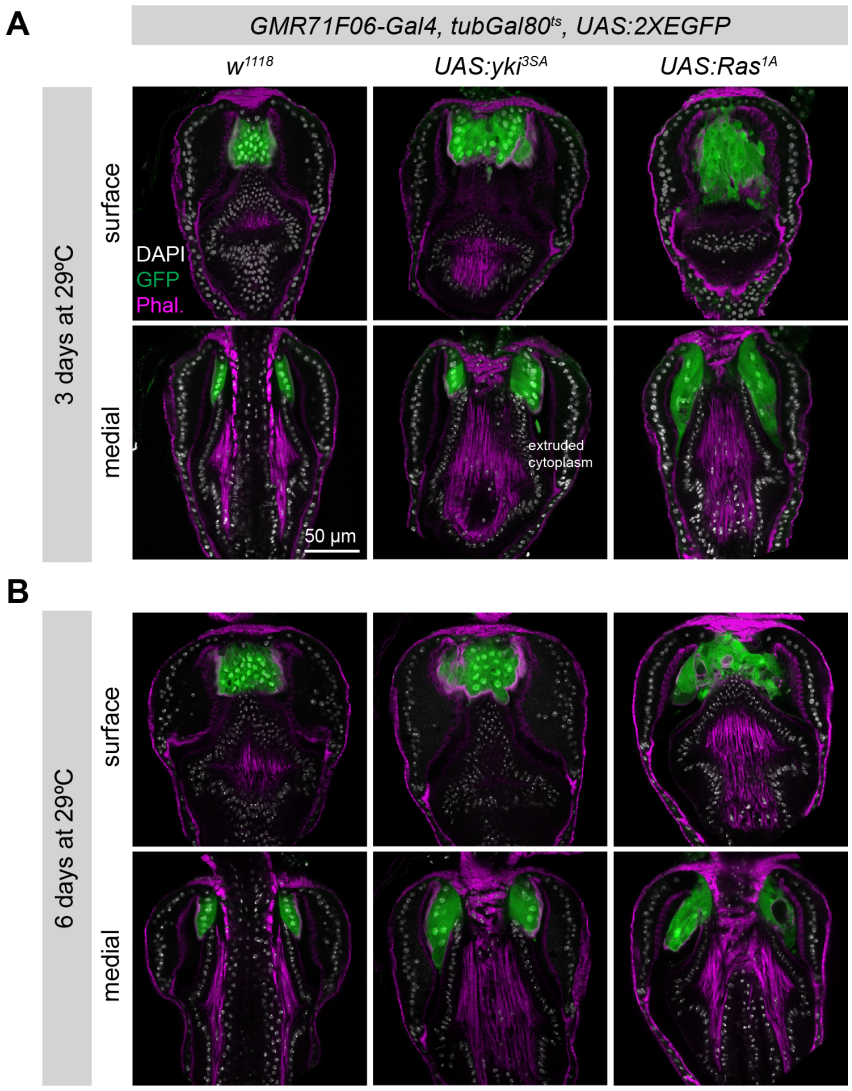

Supplemental Figure 4. Phenotypes of ectopic oncogene expression in Zone 4 cells. Ectopic expression of oncogenes *yki*^{3SA} or *Ras*^{1A} in Zone 4 cells of the proventriculus for either (A) three days or (B) six days leads to enlarged, distended tissue morphologies. These enlarged structures can be seen extruding cytoplasm into the gut lumen, and in no cases were cells observed to be growing into adjacent zones.

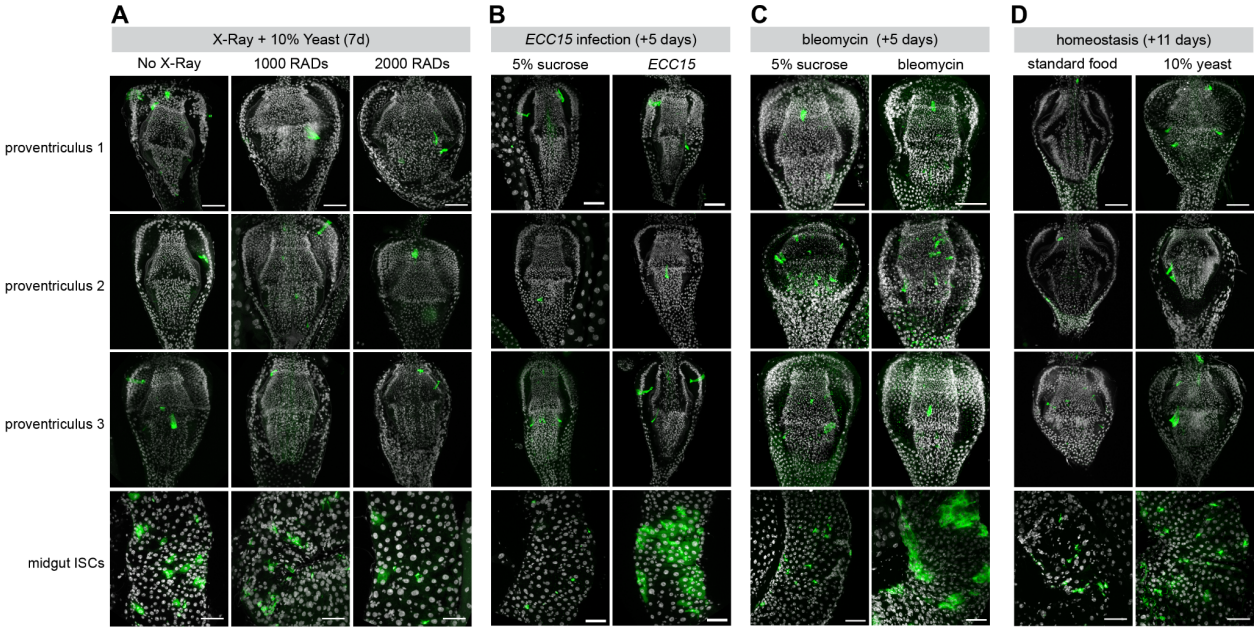

Supplemental Figure 5. MARCM analysis in the proventriculus following gut damage. Analysis of MARCM clones in the proventriculus and midgut following a number of experimental perturbations to the gut. Three representative proventriculus images are shown for each condition, from a total sample size between 10 and 23 guts. (A) X-ray damage to entire flies at 1000 or 2000 RADS, examined seven days after damage. (B) Gut damage from *ECC15* bacteria, examined 5 days after damage. (C) Gut damage from bleomycin, examined 11 days after damage. (D) Undamaged guts, fed with food supplemented with 10% yeast. Anterior is up, scale bar is 50μm.

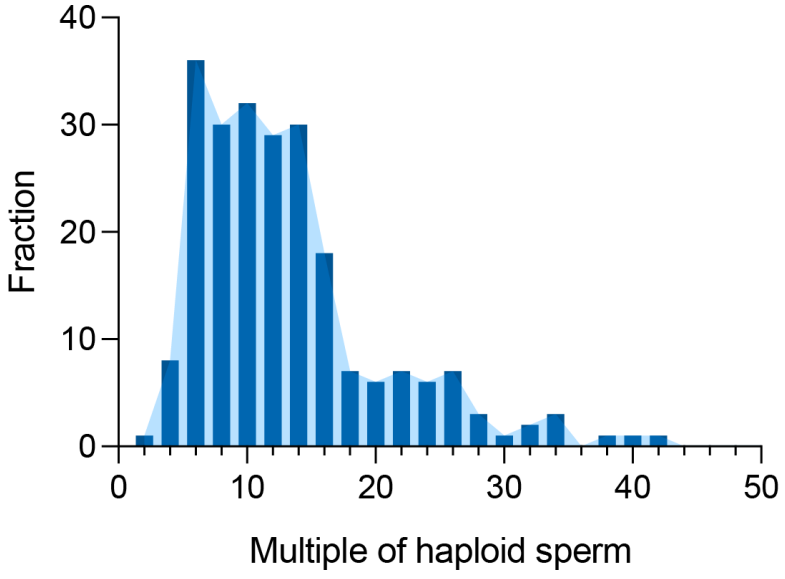

Supplemental Figure 6. Ploidy analysis of Zone 4 nuclei. Histogram of estimated ploidy of Zone 4 nuclei (n = 230 nuclei) normalized to haploid sperm nuclei.

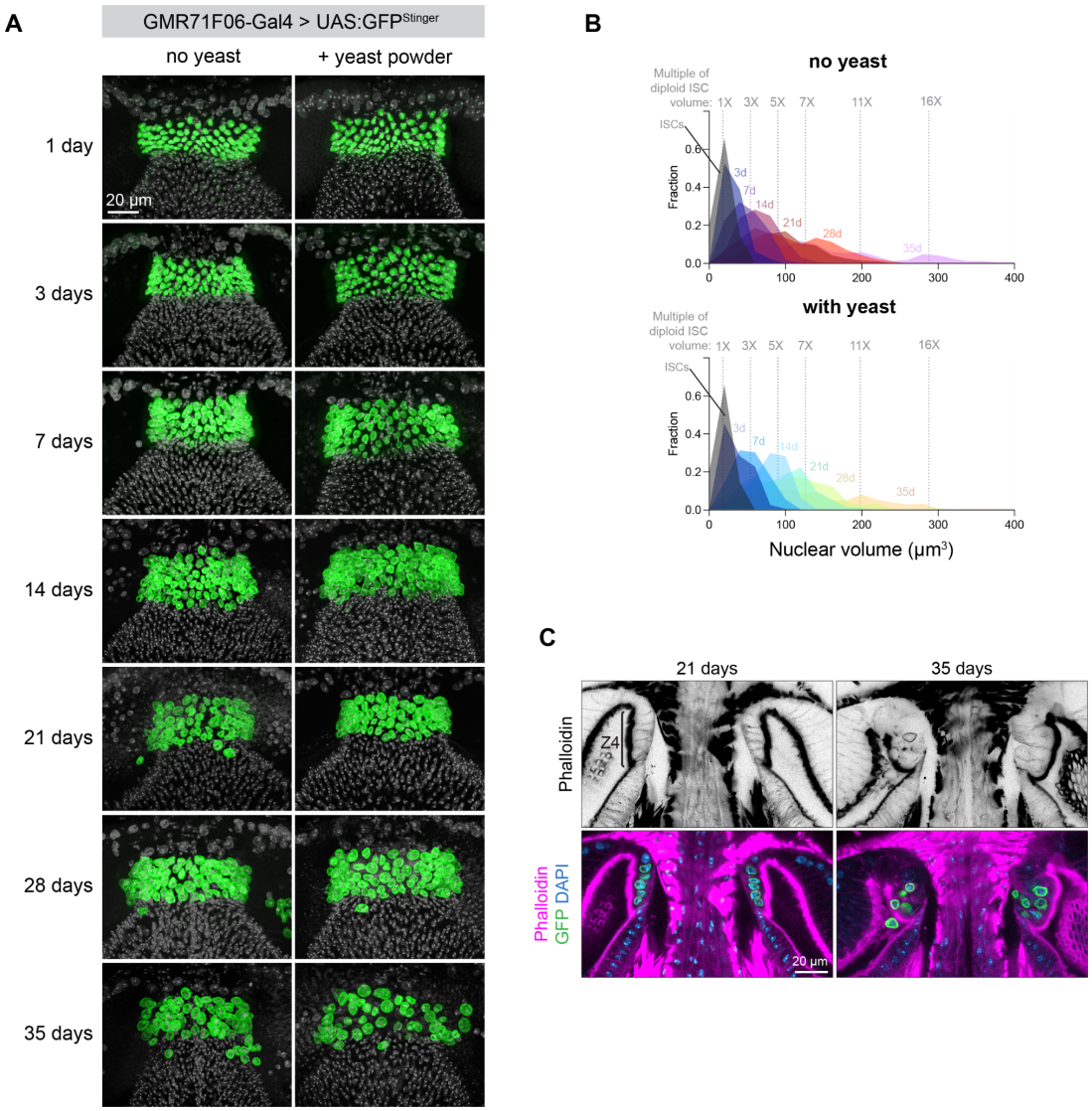

Supplemental Figure 7. Time course analysis of nuclear volume and morphology in Zone 4 cells. (A) Representative images of each time-point for the experiment shown in Figure 7. (B) Histogram of nuclear volume calculated from the data represented in Figure 7.

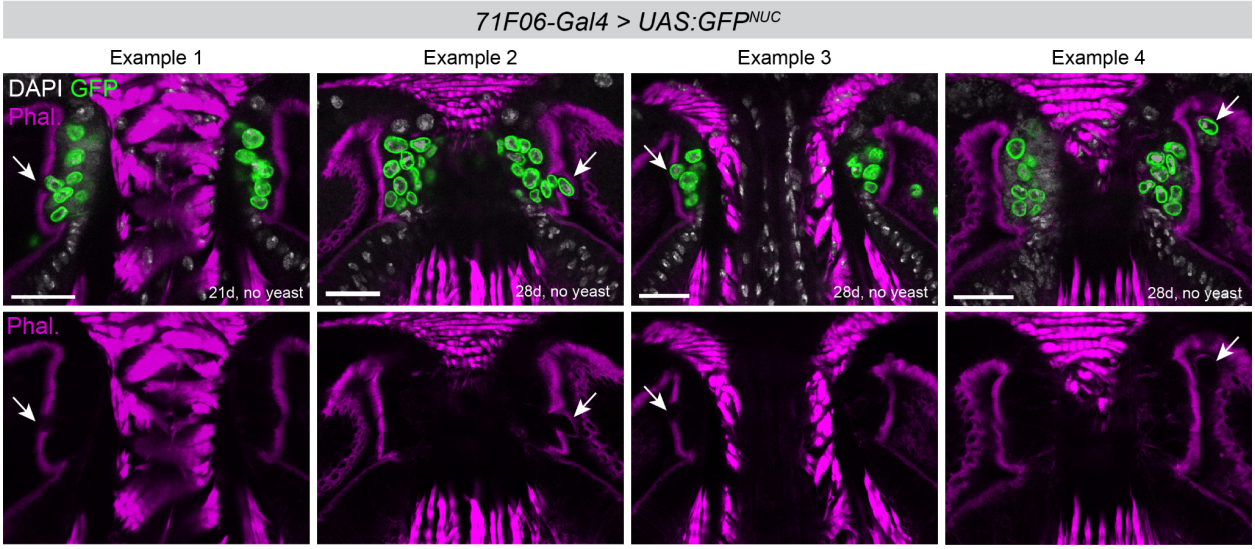

Supplemental Figure 8. Additional examples of Zone 4 nuclei loss into the gut lumen. In aging flies, GFP+ nuclei can be seen shed into the gut lumen from Zone 4. Multiple examples are shown of these nuclei appearing to exit Zone 4 via disrupted cell barriers, visible as loss of phalloidin, as well as blebs on the lumen-facing surface of Zone 4. Cells are observed at various locations along the anterior-posterior axis of Zone 4. Anterior is up, scale bar is 20μm.

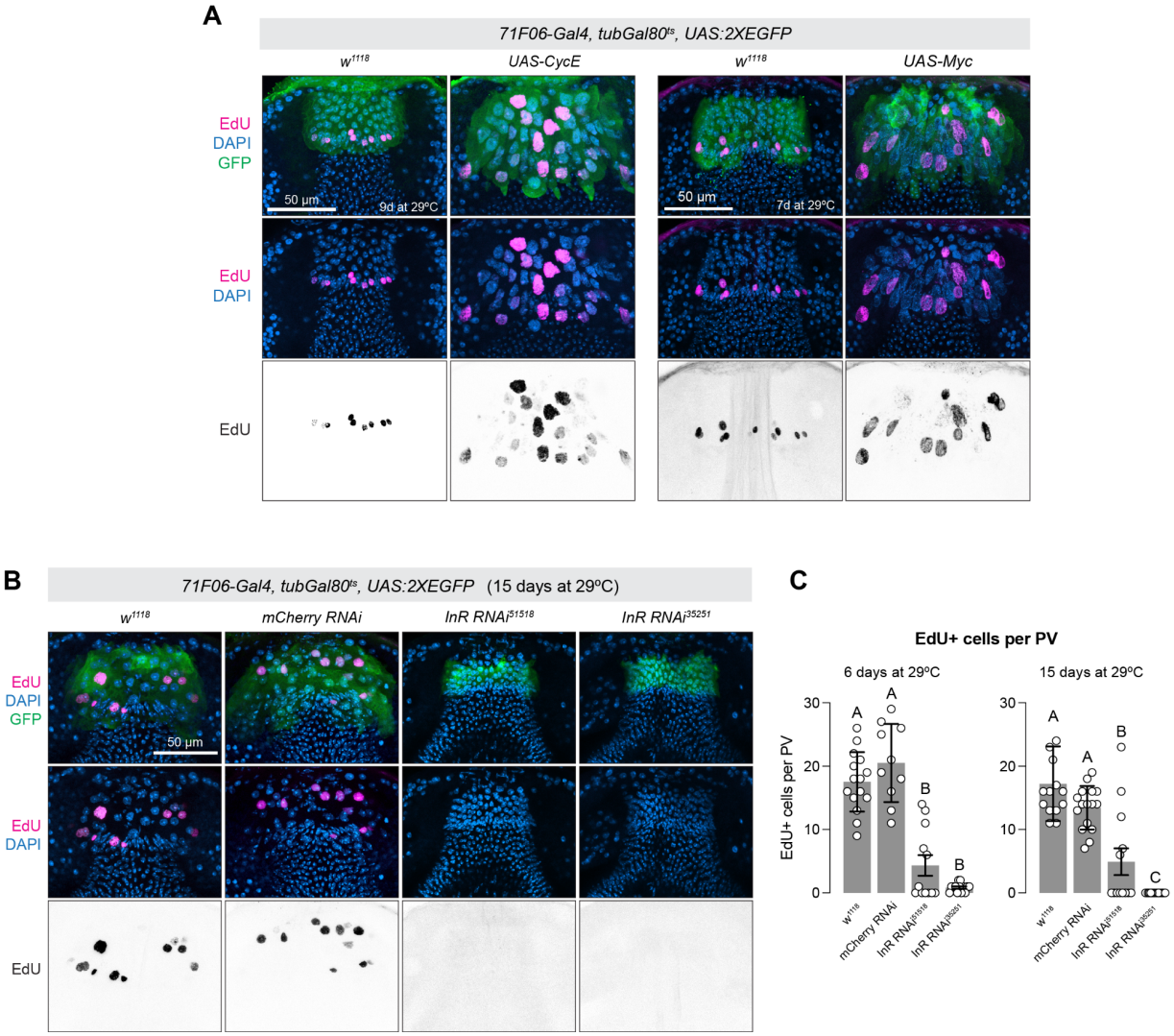

Supplemental Figure 9. Additional characterization of genetic manipulations to endocycling in Zone 4. (A) Over-expression of CycE (left) or Myc (right) leads to increased endocycling and enlargement of nuclei, as well as increased overall tissue size. Flies were fed EdU for two days prior to dissection. (B) RNAi against *InR* in Zone 4 abolishes cycling in these cells, evidenced by a lack of EdU staining and smaller nuclear size. (C) Quantification of EdU+ cells in *InR* RNAi proventrici after 6 days and 15 days at 29ºC. Letters indicate statistical significance groups (one-way ANOVA with Dunnett's multiple comparisons test.) All images are maximum intensity projections of confocal z-stacks.

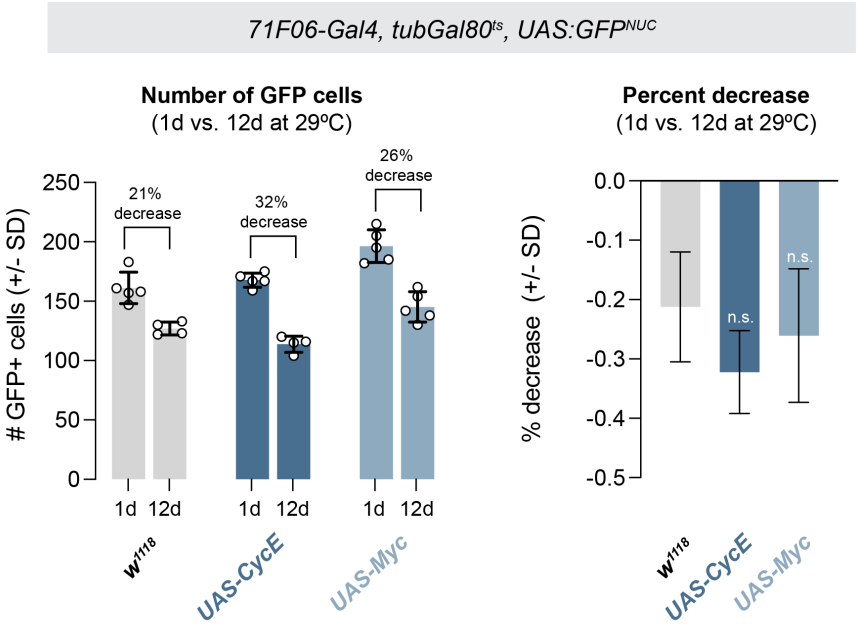

Supplemental Figure 10. Increased endocycling does not enhance cell loss in Zone 4. Left: Cell counts of GFP+ Zone 4 cells after 1 day or 12 days at 29ºC for the indicated genotypes. Right: the average percentage decrease, calculated from the data shown on the left, was not significantly different between these conditions. Error bars represent standard deviation propagated through the calculation of percentage decrease, and mean differences were compared using a t-test.

1132 **Table S1: Genotypes used in this study**

1133

1134

Figure	Genotype	Source Notes
1B, left	*yw ; + / wg[Sp-1] ; TI{GFP[3xP3.cLa]=CRIMIC.TG4.0}Chs2[CR60212-TG4.0] / P{w[+mC]=UAS-2xEGFP}AH3*	Chs2-Gal4: BL93534; UAS:2xEGFP: BL60293
1B, middle	*w ; P{w[+mC]=UAS-2xEGFP}AH2 ; P{w[+mW.hs]=GawB}Lk6[NP0101] / P{y[+t7.7] v[+t1.8]=VALIUM20-mCherry.RNAi}attP2*	"Cardia-Gal4": Kyoto DGRC 103522; UAS:2xEGFP: BL60292; mCherry RNAi: BL35785
1B, right	*w[1118] ; esg-Gal4, UAS:GFP, tubGal80[ts]*	Perrimon lab stock
1C, left	*w[1118] ; esg-Gal4, UAS:GFP, tubGal80[ts]*	Perrimon lab stock
1C right	*w[1118]; P{w[+mC]=10XStat92E-GFP}1*	Perrimon lab stock
1D	*Oregon R*	
1F	*Oregon R*	
1G	*w[1118] ; esg-Gal4, UAS:GFP, tubGal80[ts]*	Perrimon lab stock
2A	*w ; P{UAS-Stinger}2 / + ; P{y[+t7.7] w[+mC]=GMR71F06-GAL4}attP2 / MKRS*	UAS-Stinger: BL90920, GMR71F06-Gal4: BL39596
2E	*yw ; wg[Sp-1] / + ; Mi{Trojan-GAL4.0}Elovl7[MI01455-TG4.0] / P{w[+mC]=UAS-2xEGFP}AH3*	Elovl7-Gal4: BL67431
2E	*yw ; wg[Sp-1] / + ; TI{GFP[3xP3.cLa]=CRIMIC.TG4.2}CG11550[CR02741-TG4.2] / P{w[+mC]=UAS-2xEGFP}AH3*	CG11550-Gal4: BL97589
2E	*yw ; P{y[+t7.7] w[+mC]=Tub-GAL4.C-int}attP40 / + ; TI{RFP[3xP3.PB]=2A-GAL4(1-20)::N-int}Ppn[G4-N-int] / P{w[+mC]=UAS-2xEGFP}AH3*	Ppn-C-int: BL602730; tub-Gal4-C-int: BL602738
2E	*yw ; wg[Sp-1] / + ; TI{GFP[3xP3.cLa]=CRIMIC.TG4.2}Lgr1[CR01685-TG4.2] / P{w[+mC]=UAS-2xEGFP}AH3*	Lgr1-Gal4: BL86491
2E	*yw ; y[1] w[*]; Mi{Trojan-GAL4.2}Wnt4[MI03717-TG4.2] / wg[Sp-1] ; P{w[+mC]=UAS-2xEGFP}AH3*	Wnt4-Gal4: BL67449
2E	*yw ; TI{GFP[3xP3.cLa]=CRIMIC.TG4.2}Ca-Ma2d[CR01742-TG4.2] / wg[Sp-1] ; P{w[+mC]=UAS-2xEGFP}AH3*	Ca-Ma2d-Gal4: BL86499
2E	*w[*] TI{RFP[3xP3.PB]=2A-GAL4(1-20)::N-int}Mco4[G4-N-int] ; P{y[+t7.7] w[+mC]=Tub-GAL4.C-int}attP40 / + ; P{w[+mC]=UAS-2xEGFP}AH3 / +*	Mco4-N-int: BL605167; tub-Gal4-C-int: BL602738

2E	*yw ; wg[Sp-1] / + ; TI{GFP[3xP3.cLa]=CRIMIC.TG4.2}SecCl[CR01836-TG4.2]/TM3, Sb[1] Ser[1] / P{w[+mC]=UAS-2xEGFP}AH3*	SecCl-Gal4: BL91420
2E	*w ; Mex1-Gal4, UAS-2xEGFP*	Mex1-Gal4 gift of A. Petsakou (originally from Phillips & Thomas, 2006)
3A, left	*w ; P{w[+mC]=tubP-GAL80[ts]}10], P{w[+mC]=UAS-2xEGFP}AH2 ; P{y[+t7.7] w[+mC]=GMR71F06-GAL4}attP2*	GMR71F06-Gal4: BL39596, UAS:2xEGFP: BL60292, tubGal80ts: BL7108
3A, second to left	*w ; P{w[+mC]=tubP-GAL80[ts]}10], P{w[+mC]=UAS-2xEGFP}AH2 ; P{y[+t7.7] w[+mC]=GMR71F06-GAL4}attP2 / P{y[+t7.7] w[+mC]=UAS-yki.S111A.S168A.S250A.V5}attP2*	yki[3SA]: BL28817
3A, third to left	*w ; P{w[+mC]=tubP-GAL80[ts]}10], P{w[+mC]=UAS-2xEGFP}AH2 ; P{y[+t7.7] w[+mC]=GMR71F06-GAL4}attP2 / UAS:Ras[1A]*	Ras1A: gift of Chiwei Xu, Perrimon Lab
3A, fourth to left	*w ; P{w[+mC]=tubP-GAL80[ts]}10], P{w[+mC]=UAS-2xEGFP}AH2 ; P{y[+t7.7] w[+mC]=GMR71F06-GAL4}attP2*	
3A, right	*w ; P{w[+mC]=tubP-GAL80[ts]}10], P{w[+mC]=UAS-2xEGFP}AH2 ; P{y[+t7.7] w[+mC]=GMR71F06-GAL4}attP2 / P{y[+t7.7] v[+t1.8]=TRiP.HMS00001}attP2*	Notch RNAi: BL33611
4	hsFLP, FRT19A, tubGal80 / P{ry[+t7.2]=neoFRT}19A; ry[506] ; ; tub-Gal4, UAS-GFP	FRT19A: BL1709; MARCM19A: Gift of P. Jouandin
5A, top	*w ; P{w[+mC]=UAS-rpr.C}14 / + ; P{w[+mC]=tubP-GAL80[ts]}ncd[GAL80ts-7] / +*	UAS-rpr: BL5824; tubGal80ts: BL7018
5A, bottom	*w ; P{w[+mC]=UAS-rpr.C}14 / TI{GFP[3xP3.cLa]=CRIMIC.TG4.2}Ca-Ma2d[CR01742-TG4.2] ; P{w[+mC]=tubP-GAL80[ts]}ncd[GAL80ts-7] / +*	Elovl7-Gal4: BL67431
5B, top	*w ; P{w[+mC]=UAS-rpr.C}14 / + ; P{w[+mC]=tubP-GAL80[ts]}ncd[GAL80ts-7] / +*	
5B, bottom	*w ; P{w[+mC]=UAS-rpr.C}14 / + ; P{w[+mC]=tubP-GAL80[ts]}ncd[GAL80ts-7] / TI{GFP[3xP3.cLa]=CRIMIC.TG4.2}CG11550[CR02741-TG4.2]*	CG11550-Gal4: BL97589
5C, top	*w ; P{w[+mC]=UAS-rpr.C}14 / + ; P{w[+mC]=tubP-GAL80[ts]}ncd[GAL80ts-7] / +*	
5C, bottom	*w ; P{w[+mC]=UAS-rpr.C}14 / + ; P{w[+mC]=tubP-GAL80[ts]}ncd[GAL80ts-7] / Mi{Trojan-GAL4.0}Elovl7[MI01455-TG4.0]*	Ca-Ma2d-Gal4: BL86499

6A, left	*w ; P{y[+t7.7] w[+mC]=GMR71F06-GAL4.C-int}attP40 / P{w[+mC]=UAS-2xEGFP}AH2 ; P{y[+t7.7] w[+mC]=Tub-GAL4.C-int}attP2*	GMR71F06-Gal4-C-int: This manuscript
6A, middle	*w ; P{y[+t7.7] w[+mC]=Tub-GAL4.C-int}attP40 ; TI{RFP[3xP3.PB]=2A-GAL4(1-20)::N-int}Delta[G4-N-int] / P{w[+mC]=UAS-2xEGFP}AH3*	Delta-Gal4-N-int: BL602717
6A, right	*w ; P{y[+t7.7] w[+mC]=GMR71F06-GAL4.C-int}attP40 / P{w[+mC]=UAS-2xEGFP}AH2 ; TI{RFP[3xP3.PB]=2A-GAL4(1-20)::N-int}Delta[G4-N-int]*	
6B	*w ; P{y[+t7.7] w[+mC]=GMR71F06-GAL4.C-int}attP40 / P{w[+mC]=UAS-2xEGFP}AH2 ; TI{RFP[3xP3.PB]=2A-GAL4(1-20)::N-int}Delta[G4-N-int]*	
6C	*w ; P{y[+t7.7] w[+mC]=GMR71F06-GAL4.C-int}attP40 / w ; P{y[+t7.7] w[+mC]=GMR71F06-GAL4.C-int}attP40 / P{w[+mC]=UAS-2xEGFP}AH2 ; TI{RFP[3xP3.PB]=2A-GAL4(1-20)::N-int}Delta[G4-N-int] ; TI{RFP[3xP3.PB]=2A-GAL4(1-20)::N-int}Delta[G4-N-int] / P{w[+mC]=tubP-GAL80[ts]}ncd[GAL80ts-7]*	GTRACE: BL28280
7	*w ; P{UAS-Stinger}2 / + ; P{y[+t7.7] w[+mC]=GMR71F06-GAL4}attP2 / MKRS*	UAS-Stinger: BL90920, GMR71F06-Gal4: BL39596
8A, left	*w ; P{UAS-Stinger}2, P{w[+mC]=tubP-GAL80[ts]}10] / + ; P{y[+t7.7] w[+mC]=GMR71F06-GAL4}attP2 / +*	
8A, middle	*w ; P{UAS-Stinger}2, P{w[+mC]=tubP-GAL80[ts]}10] / + ; P{y[+t7.7] w[+mC]=GMR71F06-GAL4}attP2 / P{w[+mC]=UAS-CycE.L}ML1*	UAS-CycE: BL4781
8A, right	*w ; P{UAS-Stinger}2, P{w[+mC]=tubP-GAL80[ts]}10] / + ; P{y[+t7.7] w[+mC]=GMR71F06-GAL4}attP2 / M{w[+mC]=UAS-Myc.HA.WT}ZH-86Fb*	UAS-Myc: BL64759
8C, left	*w ; P{w[+mC]=tubP-GAL80[ts]}10], P{w[+mC]=UAS-2xEGFP}AH2 ; P{y[+t7.7] w[+mC]=GMR71F06-GAL4}attP2 / +*	
8C, second to left	*w ; P{w[+mC]=tubP-GAL80[ts]}10], P{w[+mC]=UAS-2xEGFP}AH2 ; P{y[+t7.7] w[+mC]=GMR71F06-GAL4}attP2 / P{y[+t7.7] v[+t1.8]=VALIUM20-mCherry.RNAi}attP2*	mCherry RNAi: BL35785
8C, second to right	*w ; P{w[+mC]=tubP-GAL80[ts]}10], P{w[+mC]=UAS-2xEGFP}AH2 / P{y[+t7.7] v[+t1.8]=TRiP.HMS03166}attP40 ; P{y[+t7.7] w[+mC]=GMR71F06-GAL4}attP2 / +*	InR RNAi: BL51518

8C, right	*w ; P{w[+mC]=tubP-GAL80[ts]}10], P{w[+mC]=UAS-2xEGFP}AH2 ; P{y[+t7.7] w[+mC]=GMR71F06-GAL4}attP2 / P{y[+t7.7] v[+t1.8]=TRiP.GL00139}attP2*	InR RNAi: BL35251
8D	Same as 8C, except UAS-Stinger instead of UAS-2xEGFP	
S1	*Oregon R*	
S2A, left	*w ; esg-Gal4, UAS:GFP, tubGal80[ts] ; +*	
S2A, right	*w ; esg-Gal4, UAS:GFP, tubGal80[ts] ; P{y[+t7.7] w[+mC]=UAS-yki.S111A.S168A.S250A.V5}attP2*	
S2C	*w ; esg-Gal4, UAS:GFP, tubGal80[ts] ; +*	
S2C	*w ; esg-Gal4, UAS:GFP, tubGal80[ts] ; UAS:Impl2*	UAS:ImpL2: Gift of Ying Liu
S2C	*w ; esg-Gal4, UAS:GFP, tubGal80[ts] / UAS:upd3 ; +*	UAS:upd3: Gift of Ying Liu
S2C	*w ; esg-Gal4, UAS:GFP, tubGal80[ts] / UAS:upd3 ; UAS:Impl2*	UAS:Impl2; UAS:upd3; Gift of A. Petsakou
S2D	*w ; dMef2-Gal4 / + ; tubGal80[ts] / +*	dMef2-Gal4: Perrimon Lab stock
S2D	*w ; dMef2-Gal4 / UAS:Impl2 ; tubGal80[ts] / +*	UAS:ImpL2: Gift of Ying Liu
S2D	*w ; dMef2-Gal4 / + ; tubGal80[ts] / UAS:upd3*	UAS:upd3: Gift of Ying Liu
S2D	*w ; dMef2-Gal4 / UAS:upd3 ; tubGal80[ts] / UAS:Impl2*	UAS:Impl2; UAS:upd3; Gift of A. Petsakou
S3	hsFLP, FRT19A, tubGal80 / P{ry[+t7.2]=neoFRT}19A; ry[506] ; ; tub-Gal4, UAS-GFP	FRT19A: BL7109; MARCM19A: Gift of P. Jouandin
S4, left	*w ; P{w[+mC]=tubP-GAL80[ts]}10], P{w[+mC]=UAS-2xEGFP}AH2 ; P{y[+t7.7] w[+mC]=GMR71F06-GAL4}attP2*	GMR71F06-Gal4: BL39596, UAS:2xEGFP: BL60292, tubGal80ts: BL7108
S4, middle	*w ; P{w[+mC]=tubP-GAL80[ts]}10], P{w[+mC]=UAS-2xEGFP}AH2 ; P{y[+t7.7] w[+mC]=GMR71F06-GAL4}attP2 / P{y[+t7.7] w[+mC]=UAS-yki.S111A.S168A.S250A.V5}attP2*	yki[3SA]: BL28817
S4, right	*w ; P{w[+mC]=tubP-GAL80[ts]}10], P{w[+mC]=UAS-2xEGFP}AH2 ; P{y[+t7.7] w[+mC]=GMR71F06-GAL4}attP2 / Ras[1A]*	Ras1A: gift of Chiwei Xu, Perrimon Lab

S5	*w ; P{UAS-Stinger}2 / + ; P{y[+t7.7] w[+mC]=GMR71F06-GAL4}attP2 / MKRS*	UAS-Stinger: BL90920, GMR71F06-Gal4: BL39596
S6	*w ; P{UAS-Stinger}2 / + ; P{y[+t7.7] w[+mC]=GMR71F06-GAL4}attP2 / MKRS*	UAS-Stinger: BL90920, GMR71F06-Gal4: BL39596
S7	*w ; P{UAS-Stinger}2 / + ; P{y[+t7.7] w[+mC]=GMR71F06-GAL4}attP2 / MKRS*	
S8	*w ; P{UAS-Stinger}2 / + ; P{y[+t7.7] w[+mC]=GMR71F06-GAL4}attP2 / MKRS*	
S9,S10	See Figure 8.	

1135